RECOMBINATION AND IONIZATION IN NARROW GAP SEMICONDUCTORS

A.V. DMITRIEV [a], **M. MOCKER** [b]

[a] *Department of Low Temperature Physics, Faculty of Physics,*
M.V. Lomonosov Moscow State University, Moscow, 119899, Russian Federation
[b] *Institute of Theoretical Physics, Physics Department, Humboldt University, Invalidenstr. 110,*
10099 Berlin, Germany

Recombination and ionization in narrow gap semiconductors

A.V. Dmitriev[a], M. Mocker[b]

[a] Department of Low Temperature Physics, Faculty of Physics, M.V. Lomonosov Moscow State University, Moscow, 119899, Russian Federation

[b] Institute of Theoretical Physics, Physics Department, Humboldt University, Invalidenstr. 110, 10099 Berlin, Germany

Contents

1. Introduction

Studies of electron–hole recombination in semiconductors are mainly stimulated by extensive use of these materials for manufacturing of detectors and as sources of radiation of different wavelength regions. This statement holds also for narrow gap semiconductors, different kinds of which are widely used in infrared devices.

Simultaneously, investigation of interband carrier transitions, recombination and impact ionization, form an important part of the physics of hot electrons in narrow gap semiconductors. Indeed, because the gap is small and the electron mobility is high, even a relatively low electric field may heat carriers up to energies of the order of ε_g, the gap width. For example, in extremely narrow gap $Bi_{1-x}Sb_x$ alloys, a field of the order of $10\,V/cm$ is sufficient [28]. High-energy carriers initiate interband impact ionization, i.e. electron transitions from the valence band to the conduction band which result in interband breakdown. In the post-breakdown regime, electron and hole concentrations and, in some cases, even the shape of the carrier distribution functions [102] are determined by the balance of generation and recombination processes in non-equilibrium conditions. One can say that it is the connection between the carrier heating process and the interband transitions that distinguishes the hot electron problem in narrow gap semiconductors from a similar problem in more traditional materials. Hence the study of interband transitions is important for many aspects of the physics of non-equilibrium phenomena in narrow gap semiconductors.

Recombination mechanisms in narrow gap semiconductors were, and remain, extensively studied (see references below). We will concentrate here mainly on the results obtained during the last fifteen years. A review of the earlier works can be found in [98].

The main processes that lead to a decrease in the excess non-equilibrium carrier concentration in narrow gap materials are generally the same as that in other semiconductors. They are Auger recombination, radiative transitions and Shockley–Read recombination, i.e. carrier capture by the local levels that are connected with impurities and lattice defects.

As a rule, Auger transitions manifest themselves in narrow gap materials in the temperature interval of intrinsic conductivity, or in the case of high doping. The higher the carrier density and temperature and the smaller the gap, the higher is the Auger transition rate. In materials having a relatively wider gap, radiative recombination may play a noticeable role. At low temperatures when electron energy diminishes and intrinsic carriers are frozen out, the lifetimes of the non-equilibrium electrons and holes are often determined by the Shockley–Read recombination.

Regarding the theory of these mechanisms, Auger recombination in narrow gap semiconductors has been studied in more detail. It has interesting specific features in both the main groups of narrow gap materials, namely, in those with Kane band structure such as $Hg_{1-x}Cd_xTe$ and also in the many-valley ones ($Pb_{1-x}Sn_xTe$, $Bi_{1-x}Sb_x$, etc.). On the contrary, the theory of impurity recombination in narrow gap semiconductors has so far attracted considerably less attention.

Nowadays there is an increased interest in artificial semiconductor structures, quantum wells and wires, superlattices, and so on. These structures, prepared from narrow gap materials, are very promising for infrared device fabrication. We will discuss the peculiarities of the interband transition processes in these structures.

We will also present existing research material that concerns the processes of impact ionization in narrow gap semiconductors.

For both recombination and generation processes, we will consider existing theoretical approaches to the transition rate calculation as well as important experimental results for the main types of narrow gap materials and their artificial structures. According to our research interests, we will pay attention to the theoretical aspects; readers interested primarily in the details of the experimental methods or in the technological problems can find the relevant information in the recent review articles [86, 119], respectively.

We will first discuss the general features of some important interband transition mechanisms and then turn to the peculiarities of these processes in the main classes of narrow gap materials. In this review, we will discuss $Hg_{1-x}Cd_xTe$, and many-valley narrow gap semiconductors will be considered in a following review.

2. Auger transitions

2.1. Auger recombination

Initially, the Auger process was introduced in atomic physics by Auger in 1925 as a non-radiative relaxation channel of an electron that has been excited from an inner atomic shell to an outer level. In this mechanism, one of the electrons from the outer shells drops down to the vacant position and the transition energy is transferred to another electron that is excited to the continuous spectrum. As a result, the atom becomes ionized.

In semiconductor physics, Auger recombination is also connected with electron–electron interaction and energy transfer to a current carrier. As the carriers can belong to different bands, and in the case of degenerate bands also to different branches and different extrema of the bands, there are different kinds of Auger transitions. For example, in Figs. 1 and 2 two important transitions are shown, the so-called eeh and ehh processes. They are often referred to as the Auger 1 and Auger 7 transitions, respectively, according to an early classification [14]. In the eeh process, the recombination energy is transferred to an electron, so that two electrons and a hole take part in the transition (in the initial state). In the ehh transition, one electron and two holes are present before the recombination and a hole takes the transition energy. In both cases the electron–hole pair disappears after the transition, which is the recombination itself, and one high-energy carrier, either an electron or a hole, remains.

The Auger transitions are very important in narrow gap materials because the efficiency of this recombination channel in a semiconductor sharply increases as ε_g diminishes. In the simplest case of the classical carrier statistics, the Auger recombination rate R is proportional to the cube of the carrier density, because three particles have to collide for the Auger transition, the electron and the hole that recombine and an additional carrier which takes the recombination energy. Then for an intrinsic semiconductor

$$R \sim n_i^3 \, ,$$

where n_i is the intrinsic electron concentration. As $n_i \sim \exp(-\varepsilon_g/2T)$, one obtains

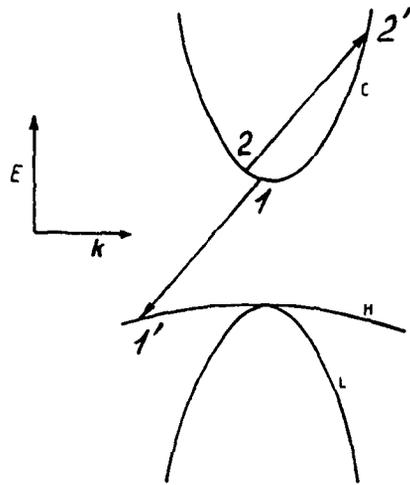$$R \sim \exp(-3\varepsilon_g/2T) \, .$$

Fig. 1. Eeh Auger recombination process (Auger 1 transition according to the classification in Ref. [14]). The transition energy is transferred to an electron in the conduction band. The bands C, H and L are the conduction, heavy-hole and light hole bands, respectively [15].
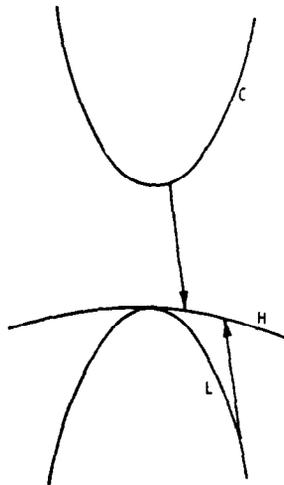
Fig. 2. Ehh recombination process (Auger 7 transition according to the classification in Ref. [14]). The transition energy is transferred to a hole in the valence band [15].

On the other hand, the radiative transition rate is proportional to the product of the electron and hole concentrations $np \sim n_i^2 \sim \exp(-\varepsilon_g/T)$ and the rate of the Shockley–Read recombination is linear in the carrier density $n \sim n_i \sim \exp(-\varepsilon_g/2T)$. So the Auger rate increases most rapidly as ε_g diminishes in comparison with the rates of the other recombination mechanisms and hence Auger recombination often dominates in narrow gap semiconductors; the smaller the energy gap

and the higher the carrier density, the more effective is this channel. The limiting value of the Auger lifetime that can be approached as $\varepsilon_g \to 0$ is rather high, being of order of the intraband electron–electron free time because the Auger process is essentially an interband carrier–carrier collision and there is no principal physical difference between inter- and intraband electron collisions if ε_g is less than the mean carrier energy.

In addition, the Auger process is an intrinsic one and hence it is always present in the material. We will now discuss it in detail.

The probability of the Auger transition can be easily written using the perturbation method of quantum mechanics, which was first performed in the pioneering work of Beattie and Landsberg [16]. For definiteness, let us consider an eeh process as shown in Fig. 1. Ehh transitions can be handled in a similar way but the particle that gets the energy is not an electron but a hole in this transition. Treating the Coulomb intercarrier interaction as a perturbation and describing the carrier wave functions by Bloch waves, one easily obtains the following expression for the probability of two particle transition from states 1 and 2 to states 1' and 2':

$$W(k_1, k_2 \to k_1', k_2')$$

$$= \frac{2\pi}{\hbar} \overline{\left| \langle k_1, k_2 | \frac{e^2}{\kappa | r_1 - r_2 |} | k_1', k_2' \rangle \right|^2} \delta(\varepsilon(k_1) + \varepsilon(k_2) - \varepsilon(k_1') - \varepsilon(k_2'))$$

$$= \frac{2\pi}{\hbar} \frac{(2\pi\hbar)^3}{2} \left[2 \left(\frac{4\pi e^2}{\kappa(k_1 - k_1')} \right)^2 I_{\text{inter}}(k_1, k_1') I_{\text{intra}}(k_2, k_2') \right.$$

$$\left. - 2 \frac{4\pi e^2}{\kappa | k_1 - k_1' |} \frac{4\pi e^2}{\kappa | k_1 - k_2' |} D(k_1, k_2, k_1', k_2') \right]$$

$$\times \delta(k_1 + k_2 - k_1' - k_2') \delta(\varepsilon_1 + \varepsilon_2 - \varepsilon_1' - \varepsilon_2') . \tag{1}$$

Here k_i is the carrier momentum in the state i; $\varepsilon_i \equiv \varepsilon(k_i)$ is the corresponding energy in the band that contains the state i; the energies of all the states are calculated from one and the same origin; κ is the dielectric constant; I_{inter}, I_{intra} and D are the so-called *overlap integrals* that are essentially the averaged scalar products of the Bloch amplitudes of the electron wave functions (see below). Typically, both branches are equally populated in each band. This means that one is interested, actually, only in the value of the transition probability averaged over the branches of all the bands the carriers from which take part in the transition. We denote this averaging in Eq. (1) by the bar above the square of the matrix element.

The expression for the matrix element used in Eq. (1) can be obtained in the following way. Prior to the transition the two-electron wave function has the form

$$\psi(r_1, r_2) = \frac{1}{\sqrt{2}} (\psi_{k_1, j_1}(r_1) \psi_{k_2, j_2}(r_2) - \psi_{k_1, j_1}(r_2) \psi_{k_2, j_2}(r_1)) , \tag{2}$$

where the subscripts j_1 and j_2 denote the branch of the spectrum that contains the corresponding carrier (each band consists of two branches because of Kramers degeneracy). The wave function $\psi'(r_1, r_2)$, after the collision, has a similar structure.

Taking Eq. (2) into account, one obtains the following expression for the average of the squared transition matrix element

$$
\overline{\left| \langle k_1, k_2 | \frac{e_2}{\kappa |r_1 - r_2|} | k_1', k_2' \rangle \right|^2}
$$

$$
= \frac{1}{16} \sum_{j_1, j_2, j_1', j_2'} \left| \langle \psi'(r_1, r_2) | \frac{e^2}{\kappa |r_1 - r_2|} | \psi(r_1, r_2) \rangle \right|^2
$$

$$
= \frac{1}{16} \sum_{j_1, j_2, j_1', j_2'} \frac{1}{4} \left| \langle \psi_{k_1', j_1'}(r_1) \psi_{k_2', j_2'}(r_2) - \psi_{k_1', j_1'}(r_2) \psi_{k_2', j_2'}(r_1) | \frac{e^2}{\kappa |r_1 - r_2|} \right.
$$

$$
\left. \times | \psi_{k_1, j_1}(r_1) \psi_{k_2, j_2}(r_2) - \psi_{k_1, j_1}(r_2) \psi_{k_2, j_2}(r_1) \rangle \right|^2 . \tag{3}
$$

The summation here is over the branches of all the bands involved in the process so that each j runs over two values.

It is convenient to use the Luttinger–Kohn basis and hence to substitute the following expressions for the electron wave functions

$$
\psi_{k_i, j_i}(r) = | k_i, j_i \rangle \, e^{ik_i \cdot r} \tag{4}
$$

where $| k_i, j_i \rangle$ is the vector of the expansion coefficients which represents the Bloch amplitude of the one-electron wave function in the Luttinger–Kohn basis.

After straightforward calculations one obtains, finally,

$$
\overline{\left| \langle k_1, k_2 | \frac{e^2}{\kappa |r_1 - r_2|} | k_1', k_2' \rangle \right|^2}
$$

$$
= \left(\frac{4\pi e^2}{\kappa |k_1 - k_1'|} \right)^2 \mathrm{Sp}\{\rho(k_1)\rho(k_1')\} \, \mathrm{Sp}\{\rho(k_2)\rho(k_2')\}
$$

$$
+ \left(\frac{4\pi e^2}{\kappa |k_1 - k_2'|} \right)^2 \mathrm{Sp}\{\rho(k_1)\rho(k_2')\} \, \mathrm{Sp}\{\rho(k_2)\rho(k_1')\}
$$

$$
- 2 \left(\frac{4\pi e^2}{\kappa |k_1 - k_1'|} \right) \left(\frac{4\pi e^2}{\kappa |k_1 - k_2'|} \right) \mathrm{Sp}\{\rho(k_1)\rho(k_1')\rho(k_2)\rho(k_2')\} , \tag{5}
$$

where

$$
\rho(k_i) = \tfrac{1}{2} \sum_{i_i} | k_i, i_i \rangle \langle k_i, i_i | \tag{6}
$$

is the density matrix (see, for example, Ref. [52]) describing the (mixed) electron state in a given band with a given momentum k_i, which contains the (pure) states from both branches of the band in equal portions. The sum is just over these branches. For a given momentum, density matrices are different in different bands but we omit the band indices in Eqs. (5) and (6) to simplify the notation

because it is always clear to what band the electron state under consideration belongs in the transition. Sometimes the density matrix doubled is called the projection operator on the state k_l in the corresponding band [55, 57].

As k_1 and k_2 enter symmetrically in Eq. (1), one can combine the first two terms in Eq. (5) to obtain

$$I_{\text{inter}} = \text{Sp}\{\rho(k_1)\rho(k_1')\} ,$$

$$I_{\text{intra}} = \text{Sp}\{\rho(k_2)\rho(k_2')\} , \tag{7}$$

$$D = \text{Sp}\{\rho(k_1)\rho(k_1')\rho(k_2)\rho(k_2')\} .$$

The density matrices and hence the overlap integrals can be easily found for the main models of the band structure in narrow gap semiconductors, because only a small limited number of bands is taken into account in them. This is a specific feature of narrow gap materials where the dispersion laws are formed mainly by the interaction between those several states that are separated by the narrow energy gap while the influence of the farther states can be neglected or taken into account implicitly. Correspondingly, the traces of the products of the density matrices in Eq. (5) are restricted to the summation over the same finite set of states.

If the valence band is degenerate as in $Hg_{1-x}Cd_xTe$, different Auger transitions are possible (see Fig. 4), and different interband overlap integrals correspond to them depending upon the spectrum branches between which the carrier that takes the energy performs the transition. Expressions for different overlap integrals as well as the method of their calculation can be found in the appendix.

The calculations presented above show that the structure of the carrier wave functions reflects significantly in the structure of the transition probability W. First, the two terms in braces in the third line of Eq. (1) come from the direct (Coulomb) and exchange transitions that appear due to the antisymmetry condition for the two-electron wave functions (see Eq. (2)). Second, the exponential factors $e^{ik \cdot r}$ in the one-particle wave functions result in the momentum conservation law. And third, the overlap integrals I_{inter} and I_{intra} are the matrix elements squared of the Bloch amplitudes of the one-particle wave functions, averaged over band indices as described above. These matrix elements are taken between the states of the recombining pair for I_{inter}, and between the states of the particle that gets the energy, before and after the transition, for I_{intra}. In D, the same matrix elements are combined in a similar but slightly more complicated way. Umklapp processes were neglected in Eq. (1).

To find the total recombination rate, one should integrate the transition probability W over all initial and final states $1, 1', 2$ and $2'$ of the particles, including appropriate statistical factors to take into account also the probability that the initial states are filled by electrons and the final ones are empty:

$$R = \frac{2\pi}{\hbar} \int \frac{8}{(2\pi\hbar)^9} \, dk_1 \, dk_2 \, dk_1' \, dk_2' \left[2\left(\frac{4\pi e^2}{\kappa(k_1 - k_1')}\right)^2 I_{\text{inter}}(k_1, k_1') I_{\text{intra}}(k_2, k_2') \right.$$

$$\left. - 2 \frac{4\pi e^2}{\kappa|k_1 - k_1'|} \frac{4\pi e^2}{\kappa|k_1 - k_2'|} D(k_1, k_2, k_1', k_2') \right] P_r \delta(\textstyle\sum k) \delta(\textstyle\sum \varepsilon) , \tag{8}$$

$$P_r = f_1 f_2 (1 - f_1')(1 - f_2') \, . \tag{9}$$

Here P_r is the so-called statistical factor, $f_i \equiv f(k_i)$ is the electron distribution function, i.e. the probability that the state i is occupied by an electron, so that $(1 - f)$ is the distribution function for holes.

The multi-dimensional integral (8) is, in general, extremely difficult to calculate. Indeed, even after integration over three momentum components with the help of the momentum conservation law, the remaining integration is still over the eight-dimensional hyper-surface that is given by the energy conservation condition in the nine-dimensional k-space. Symmetry arguments may further reduce the number of variables, but the resulting dimension of the integral remains high, being typically equal to 5 or 6. In a general case, when carrier distributions are degenerate and the mean electron energies are comparable to ε_g, there is no other method for the evaluation of the rate integral except for direct numerical calculations [110, 44, 80, 88] that are rather complicated and very time-consuming.

There is, however, an important limiting case when the Auger rate calculations can be performed analytically [16]. Indeed, let us assume that the carrier distributions are non-degenerate and that the temperature is low enough,

$$T \ll \varepsilon_g \, . \tag{10}$$

Then the statistical factor takes the form

$$
\begin{aligned}
P_r &= \exp\left(\frac{\zeta_1 + \zeta_2 - \zeta_1'}{T}\right) \exp\left(-\frac{\varepsilon_1 + \varepsilon_2 - \varepsilon_1'}{T}\right) \\
&= \exp\left(\frac{\zeta_1 + \zeta_2 - \zeta_1'}{T}\right) \exp\left(-\frac{\varepsilon_2'}{T}\right) ,
\end{aligned} \tag{11}
$$

where the energy conservation law has been used for the transformations. Here ζ_i is the (quasi-)Fermi level in the band that contains the state i.

One can easily see from Eqs. (11) and (8) that the major contribution to the rate comes from the transitions for which the value of ε_2' is close to its minimum. The minimum value of ε_2', $\varepsilon_{2\,min}'$, is called the threshold value, and the corresponding transition is called the threshold of the Auger process for a reason that will be clear soon. If for a transition the corresponding ε_2' value exceeds the minimum by more than a few T then its contribution to the rate integral is negligible. Hence, if in the region of the k-space that corresponds to the transitions with ε_2' close to $\varepsilon_{2\,min}'$ the matrix elements and the overlap integrals do not change significantly, one can substitute for them their values taken at the threshold thus simplifying the integral radically.

For low temperatures $T \ll \varepsilon_g$, one can always do this procedure with the Fourier transform of the Coulomb electron–electron interaction, because the momentum transfer $|k_1 - k_1'| = |k_2 - k_2'|$ that enters the matrix element is of the order of $\sqrt{m\varepsilon_{2\,min}'}$ where m is the effective mass in the band to which the high energy particle belongs. As $\varepsilon_{2\,min}'$ evidently cannot be less than ε_g, the small variation of ε_2' of the order of T will not change the momentum transfer significantly and hence the transform as a whole. The same usually also holds for the intraband overlap integral I_{intra}.

The situation may be more complicated, however, for the interband overlap integral [54, 55, 18] because for some types of band spectrum the threshold value of the integral equals zero or is very

small. I_{inter} may also depend on the angle between $\boldsymbol{k}_1$ and $\boldsymbol{k}_1'$ which is not necessarily strictly fixed by the condition $\varepsilon_2' - \varepsilon_{2\,\text{min}}' \ll \varepsilon_g$. In these cases one certainly cannot substitute a constant value for I_{inter} and should either use the precise original expression for it or some suitable expansion into the momentum series near the threshold [54, 55, 18].

To demonstrate the general idea of the approach of Beattie and Landsberg, let us assume here for simplicity that one can substitute the threshold value also for I_{inter}. We remind the reader, however, that we do it for the purpose of illustration only and that this step is incorrect for the main classes of narrow-band semiconductors. We continue to consider the eeh process so that the particles 1, 2 and 2' are within the conductivity band with the band dispersion law $\varepsilon_c(\boldsymbol{k})$, and the particle 1' is in the valence band and its dispersion relation is $\varepsilon_v(\boldsymbol{k})$. We treat all energies as energies of electrons in the corresponding bands and measure them from a common origin.

Then one immediately obtains from Eq. (8)

$$
\begin{aligned}
R &= \text{const. } \exp\left(\frac{2\zeta_c - \zeta_v}{T}\right) \int d\boldsymbol{k}\, d\boldsymbol{q}\, d\boldsymbol{k}_2' \exp\left(-\frac{\varepsilon_c(\boldsymbol{k}_2')}{T}\right) \\
&\quad \times \delta(\varepsilon_c(\boldsymbol{k}_2') - \varepsilon_c(\boldsymbol{k}_2' - \boldsymbol{q}) + \varepsilon_v(\boldsymbol{k} - \boldsymbol{q}/2) - \varepsilon_c(\boldsymbol{k} + \boldsymbol{q}/2)) \\
&= \text{const. } \exp\left(\frac{2\zeta_c - \zeta_v}{T}\right) \int d\boldsymbol{k}_2' \exp\left(-\frac{\varepsilon_c(\boldsymbol{k}_2')}{T}\right) \\
&\quad \times \int d\boldsymbol{k}\, d\boldsymbol{q}\, \delta(\varepsilon_c(\boldsymbol{k}_2') - \varepsilon_c(\boldsymbol{k}_2' - \boldsymbol{q}) \\
&\quad + \varepsilon_v(\boldsymbol{k} - \boldsymbol{q}/2) - \varepsilon_c(\boldsymbol{k} + \boldsymbol{q}/2)) \, ,
\end{aligned}
\tag{12}
$$

where new variables $\boldsymbol{k}$ and $\boldsymbol{q}$ were introduced instead of $\boldsymbol{k}_1$, $\boldsymbol{k}_1'$ and $\boldsymbol{k}_2$ to explicitly take into account the momentum conservation.

As $T \ll \varepsilon_g$, one can use parabolic approximation for the dispersion laws when calculating the concentrations and hence make use of the expressions

$$
n = N_c^*(T)\exp\left(\frac{\zeta_e - \varepsilon_{c\,\text{min}}}{T}\right) ,
$$

$$
p = N_v^*(T)\exp\left(\frac{\zeta_h - \varepsilon_{v\,\text{max}}}{T}\right) ,
\tag{13}
$$

where

$$
N_c^* = 2[m_e T / 2\pi\hbar^2]^{3/2} , \qquad N_v^* = 2[M_h T / 2\pi\hbar^2]^{3/2}
\tag{14}
$$

are the effective numbers of states in the bands, m_e and M_h being the electron and hole effective masses, respectively. Then one comes to the equality

$$
\exp\left(\frac{2\zeta_c - \zeta_v}{T}\right) = \frac{n^2 p}{(N_c^*)^2 N_v^*} \exp\left(\frac{\varepsilon_g + \varepsilon_{c\,\text{min}}}{T}\right) ,
$$

where we have taken into account that ζ_h, the Fermi energy of the holes, and ζ_v, that of the electrons in the valence band, differ by the sign, so that $\zeta_h = -\zeta_v$. Now it is possible to re-write Eq. (12) in a more familiar form with the carrier density dependence shown explicitly:

$$
R = n^2 p \frac{\text{const.}}{(N_c^*)^2 N_v^*} \int dk_2' \exp\left(-\frac{\varepsilon_c(k_2') - \varepsilon_{c\,min} - \varepsilon_g}{T} \right)
$$

$$
\times \int dk\, dq\, \delta(\varepsilon_c(k_2') - \varepsilon_c(k_2' - q) + \varepsilon_v(k - q/2) - \varepsilon_c(k + q/2)) . \tag{15}
$$

It is worth noting that R is always proportional to the cube of the particle density in the case of classical (Boltzmann) statistics because three particle 1, 2 and 1' have to collide for the Auger transition. R is proportional to $n^2 p$ for eeh process and to np^2 for the ehh one, so ehh transitions are usually more important in n-type materials and ehh ones in p-type semiconductors. Density dependence may be different, however, if the carriers are degenerate [54, 55, 62, 18, 132].

It is convenient to calculate first the inner integral in Eq. (15). As was already mentioned, for $T \ll \varepsilon_g$ the energies of the particles 1, 1' and 2, which are of the order of T, are low enough to justify the use of the parabolic approximation for their dispersion relations. Then the argument of the δ-function reduces to a bilinear function of q and k, which can be transformed to a diagonal form by a linear coordinate transformation in momentum space. After this transformation, the integration can be performed easily in the spherical coordinates [79]. Hence one obtains a function of k_2' as a value of the inner integral in Eq. (15); let this function be $Z(k_2')$. It gives in fact the phase volume allowed for all possible transitions for a given value of k_2'. Of course, Z depends on the direction of k_2' only if the carrier dispersion law is anisotropic. Evidently, Z has a non-zero value only if ε_2' is greater than $\varepsilon_{2\,min}'$, and usually Z becomes proportional to some positive power γ of $\varepsilon_2' - \varepsilon_{2\,min}'$ after averaging over different k_2' directions on the surface $\varepsilon(k_2') = \text{const.}$

Hence one now obtains

$$
R = n^2 p \frac{\text{const.}}{(N_c^*)^2 N_v^*} \exp\left(-\frac{\varepsilon_{2\,min}' - \varepsilon_{c\,min} - \varepsilon_g}{T} \right) \int_{\varepsilon_{2\,min}'}^{\infty} d\varepsilon_2'\, \rho_c(\varepsilon_2')
$$

$$
\times \exp\left(-\frac{\varepsilon_2' - \varepsilon_{2\,min}'}{T} \right) \int \frac{d\Omega_2'}{4\pi} Z(k_2')
$$

$$
= n^2 p \frac{\text{const.}}{(N_c^*)^2 N_v^*} \exp\left(-\frac{\varepsilon_{2\,min}' - \varepsilon_{c\,min} - \varepsilon_g}{T} \right) \int_0^{\infty} d\varepsilon\, \rho_c(\varepsilon_{2\,min}' + \varepsilon) \exp\left(-\frac{\varepsilon}{T} \right) \varepsilon^\gamma \tag{16}
$$

and, finally,

$$
R = C_A n^2 p ,
$$

$$
C_A = \text{const.} \left(\frac{T}{\varepsilon_g} \right)^y \exp\left(-\frac{\varepsilon_a}{T} \right) , \tag{17}
$$

$$
\varepsilon_a = \varepsilon_{2\,min}' - \varepsilon_{c\,min} - \varepsilon_g . \tag{18}
$$

C_A is called the *Auger coefficient*, and ε_a is the *activation energy* of the process. It is evident from Eq. (17) that the Auger coefficient does not depend upon carrier concentrations (we considered classical carrier statistics here; the results may be different in the degenerate case, see Section 3.2.1).

In deriving Eq. (17) from Eq. (16), we used

$$\rho_c(\varepsilon'_{2\,min} + \varepsilon) \approx \rho_c(\varepsilon'_{2\,min}) = \text{const.}$$

because $\varepsilon \sim T \ll \varepsilon'_{2\,min} \sim \varepsilon_g$.

Calculation of the outer integral over k'_2 in Eq. (16) is straightforward and gives some positive power of the temperature as a result. Actually, the interband overlap integral, which we have omitted here for simplicity, also contributes to this power. As $(N_c^*)^2 N_v$ in the denominator of Eq. (16) is in turn proportional to $T^{9/2}$, the resulting power of the temperature, y, in the pre-exponential factor may be either positive or negative. In any case, the main part of the low temperature dependence of the Auger rate is exponential with the activation energy ε_a equal to the difference between the threshold energy of the high-energy particle calculated from the corresponding band edge, and ε_g. So it is important to have a method to calculate the activation energy.

To do this, it is more convenient to look at the reverse of the Auger recombination process, i.e. the process of impact ionization produced by a high energy particle 2' in its collision with an electron 1' in the valence band. As a result, two low-energy particles 2 and 1 appear, such that the electron undergoes an interband transition from state 1' to 1. Evidently, the energy and momentum conservation laws are identical for the recombination and ionization transitions, and hence the $\varepsilon'_{2\,min}$ values coincide for them. As a result, one can calculate $\varepsilon'_{2\,min}$ as the minimum energy a carrier requires for impact ionization.

One can also consider ionization as a decay of one initial particle 2' into three particles, namely two electrons in states 1 and 2 and a hole in state 1' in the valence band (the eeh process). Hence we have here the standard problem of particle physics, namely particle decay into a set of other particles, and $\varepsilon'_{2\,min}$ is indeed the threshold energy of this process, i.e. the minimal energy for particle decay. As the decay we consider here is just the impact ionization, its threshold energy is called the *ionization threshold* and denoted $\varepsilon_I \equiv \varepsilon'_{2\,min}$.

The conditions that determine the threshold are well known (see, for example, Ref. [87]). They reduce to the equality of velocities of all particles that are born as a result of the decay, and together with the conservation laws they enable one to find the momenta of all the particles participating in this threshold transition and hence to determine $\varepsilon'_{2\,min}$. These calculations are highly sensitive to the precise shape of the band spectrum and they should be performed separately for each specific band structure. Some details of the threshold calculations and the corresponding results can be found for the Kane band model, which describes the band spectrum in $Hg_{1-x}Cd_xTe$ [55, 57], and for the Lax model, which can be used for the description of the carrier dispersion laws in many-valley narrow gap semiconductors such as $Pb_{1-x}Sn_xTe$ or $Bi_{1-x}Sb_x$ [18, 133]. The detailed description of the band dispersion law models will be given below in the material-specific sections.

The results are as follows for the Kane spectrum for eeh and ehh processes, respectively

$$\varepsilon_a^{eeh} = 2\frac{m_e}{M_h}\varepsilon_g, \qquad \varepsilon_a^{ehh} = \frac{m_e}{M_h}\varepsilon_g,$$

$$\varepsilon_I \equiv \varepsilon'_{2\,min} = \varepsilon_g + \varepsilon_a, \tag{19}$$

where m_e is the effective mass of the electron and M_h of the heavy hole, respectively. It was assumed here that $m_e \ll M_h$.

For the Lax spectrum which is essentially the anisotropic Dirac model

$$\varepsilon_a = \frac{m_t \varepsilon_g}{m_l \sin^2(\phi)} , \qquad \varepsilon_I \equiv \varepsilon'_{2\,\mathrm{min}} = \varepsilon_g + \varepsilon_a , \tag{20}$$

where m_t and m_l are the transverse and longitudinal effective masses in the valley, respectively. It was assumed here that $m_t \ll m_l$. ϕ is the angle between the axes of the equivalent valleys in the spectrum.

As $\varepsilon_a \ll \varepsilon_g$ in both cases, the activation temperature dependence of the Auger rate can be observed only in the relatively narrow interval $T < \varepsilon_a \ll \varepsilon_g$.

Let us now turn to the impact ionization process. Its probability is also given by expression (1) because according to the principle of detailed balance, the probabilities for the direct and the inverse processes coincide. Hence, Eq. (8) is also valid for the ionization rate if one substitutes the statistical factor P_i for P_r in Eq. (8):

$$P_i = f'_1 f'_2 (1 - f_1)(1 - f_2) . \tag{21}$$

The general expression obtained in this way is valid for any carrier distribution. If the distribution functions are the Fermi functions with one temperature but different quasi-Fermi levels, it is easy to show that

$$P_i = \exp\left(\frac{\zeta_v - \zeta_c}{T}\right) P_r .$$

Hence in the case of quasi-equilibrium, the rates of the Auger recombination and impact ionization differ only by the factor $\exp((\zeta_v - \zeta_c)/T)$ and coincide in the full thermodynamical equilibrium when ζ_v and ζ_c are equal. So if one is interested in quasi-equilibrium conditions only, there is no difference which quantity to calculate, and usually, the ionization rate is more convenient for calculations. The rate of either process is not zero even in equilibrium, but they compensate each other in these conditions, as it should be.

The method of Beattie and Landsberg is a convenient one and has been used in a significant part of the Auger rate calculations in narrow gap semiconductors. It is applicable, however, only in the low temperature region (see Eq. (10)). Moreover, its results may deviate extremely rapidly from the true rate values as the temperature is increased. It was found [43] that the error of the method approaches 100% at T as low as $\varepsilon_g/20$ in a material with a highly anisotropic many-valley spectrum, such as $Pb_{1-x}Sn_xTe$ or $Bi_{1-x}Sb_x$ (see Fig. 3). As far as we know, the precision of the method is yet to be investigated for the Kane band model.

A simple analytical approach to the Auger rate calculation is possible again in the limiting case that is in some sense opposite to that considered by Beattie and Landsberg, i.e., when the carriers are degenerate and their concentration is so high that $\varepsilon_F \gg \varepsilon_g$. This situation has been studied for the many-valley narrow gap semiconductor with the Lax band spectrum [18]. As in the limit $\varepsilon_F \gg \varepsilon_g$ the only parameter that determines the size of the integration area in the rate integral (8) is k_F, the Fermi momentum, one can easily find the dependence of the rate on k_F simply by
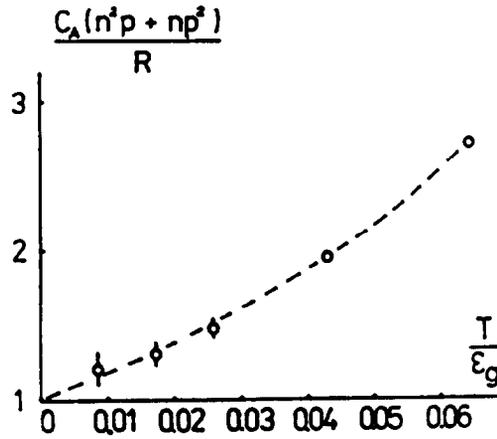
Fig. 3. The ratio of the Auger rate found analytically [18] using the method of Beattie and Landsberg to the rate calculated numerically [43].

introducing the dimensionless variables $p_i = k_i/k_F$ and removing k_F from the integral which turns into a dimensionless constant. The result is as follows

$$R \sim k_F^4 \sim n^{4/3} ,$$

where n is the carrier concentration (it was assumed that $n = p$ in Ref. [18]).

Analytical methods based on the non-equilibrium Green's function technique were also developed for Auger rate calculations in narrow gap semiconductors [131, 132, 94], but they were not as popular as the Beattie–Landsberg approach or direct numerical calculations.

2.2. Impact ionization

The basic quantity that describes the impact ionization process is the probability, $W_I(k)$, that the electron in the state k generates an electron–hole pair per unit time. The ionization probability can be expressed as

$$W_I(k) = \int \frac{8}{(2\pi\hbar)^9} \, d^3k_1 \, d^3k_1' \, d^3k_2 \, W(k_1', k \rightarrow k_1, k_2) , \qquad (22)$$

where W is given by Eq. (1). The evident property of the ionization probability $W_I(k)$ is that it can have non-zero values only if the corresponding carrier energy $\varepsilon(k)$ exceeds the ionization threshold ε_I (see Section 2.1). The total ionization rate can be expressed through W_I as

$$G = \int \frac{2 \, d^3k}{(2\pi\hbar)^3} \, f(k) W_I(k) , \qquad (23)$$

where $f(k)$ is the distribution function of the ionizing carriers.

Another important quantity is the *ionization coefficient* α, defined as the probability for ionization of an electron per unit path in the field direction. It is connected to the ionization probability through the following relation

$$\alpha(E) = \frac{1}{v_d} \int \frac{2\,d^3 k}{(2\pi\hbar)^3} f(k) W_I(k) = \frac{G}{v_d}\,, \tag{24}$$

where $v_d(E)$ is the carrier drift velocity. The *impact ionization velocity* is defined as

$$g(E) = \frac{G}{n}\,, \tag{25}$$

where n is the concentration of ionizing particles:

$$n = \int \frac{2\,d^3 k}{(2\pi\hbar)^3} f(k)\,. \tag{26}$$

One can see from Eqs. (23)–(25) that the ionization intensity depends on the shape of the distribution function of the ionizing particles. As a result, the computations for impact ionization are, in general, significantly more complicated than that of Auger recombination. Indeed, recombination is usually studied under conditions of quasi-equilibrium when the shape of the distribution functions is known (Fermi functions). On the contrary, impact ionization is studied typically in a highly non-equilibrium situation, for example in a high electric field, and the shape of the distribution function of the high energy ionizing particles is not known. The calculation of this distribution function is a complicated task, first of all because the function depends on the electron scattering processes at high energies (of order ε_g), which are often questionable, as well as the precise shape of the carrier dispersion law in this region. In addition, the very computation of the far tail of the distribution function in a high field is a complicated problem in itself. An analysis of the well-known attempts to calculate the high energy tail of the distribution function [114, 11, 108, 79, 45, 127, 109] (some recent results in this field can be found in Refs [37, 38, 105, 30, 126]) lies outside the scope of our review. We will briefly outline here only the main features that follow from these studies.

At low fields the ionizing carrier distribution in the electric field consists of very few electrons that were accelerated along the field without a single collision (Shockley's ballistic electrons). Hence the carrier distribution is highly anisotropic at these energies, looking like a sharp needle in the field direction. At higher fields one finds a more or less isotropic halo of more numerous Ridley's lucky drifting particles [108] that could avoid inelastic collisions in their movement but underwent more probable elastic (or quasi-elastic) scattering processes. The major part of the carriers is concentrated at lower energies. Their distribution is formed under the influence of both elastic and inelastic scattering processes. These electrons dominate the current.

The boundaries between these energy regions are not fixed. They depend on the carrier dispersion law, scattering mechanisms and the electric field value. So the ionization threshold may lie, generally, in any one of the regions. In insulators and wide gap semiconductors where the threshold energy is high, it usually lies, depending on the material and on the field value, in Shockley's or Ridley's region. In narrow gap materials where the ionization threshold is low it can

fall not only into these high energy intervals but also into the low-energy region even in a moderate field.

Ionization by rare carriers that belong to the far tail of the distribution function is typical for insulators and wide gap semiconductors where the ionization threshold is high. On the contrary, in zero gap semiconductors, such as HgTe or $Hg_{1-x}Cd_xTe$ alloys with $x \leq 0.16$ (at $T = 4.2$ K), the ionization threshold equals zero because ε_g is zero so that all the carriers can ionize. Correspondingly, the ionization rate is determined here by the "main body" of the distribution function or even by its low energy part [17,49]. This may simplify the calculations because the main part of the distribution function can often be found with the help of the well-known methods and under suitable approximations of the physics of hot electrons [50,106], which may not be applicable to the far tail of the distribution function. For example, the effective temperature approximation is justified in HgTe [17,93], and it has been used in Ref. [44] for analytical calculations of the impact ionization rate in this material.

The approach developed for zero gap semiconductors can also be applied to the narrow gap ones if the mean carrier energy in the applied field is greater than, of order of, or only slightly less than the ionization threshold energy. Physically, this is the high field limit, when the ionization rate becomes high. However, it does not require a very high electric field in the narrow gap materials because, on the one hand, the threshold is low for small ε_g, and on the other hand, small ε_g results in light carrier masses and hence in high mobility and low scattering rates, both factors being favourable for intense carrier heating. This approach has been applied to the calculation of the impact ionization probability in narrow gap semiconductors with the Lax spectrum such as $Pb_{1-x}Sn_xTe$ and $Bi_{1-x}Sb_x$ [18]. In this article, the carrier distribution functions were taken in the Fermi form because of the frequent electron–electron collisions (effective temperature approximation). As a result, the calculations could be performed in quasi-equilibrium conditions in full analogy to the common Auger rate computations. Gelmont's expressions for the Auger transition rates in Kane semiconductors at equilibrium [55,57] (see Eqs. (32) and (33) in Section 3.2.1) also give the impact ionization rates calculated under the same conditions, if one considers the temperature in these formulae as the effective temperature of the ionizing carriers.

If impact ionization is studied in lower fields so that the mean carrier energy is much less than ε_I, the well-known Townsend–Shockley arguments [120,114] become applicable to narrow gap semiconductors. In these situations, only the ballistic particles that could avoid collisions in their drift in the field can gain sufficient energy for ionization. Assuming the carrier mean free path l_c to be constant and small as compared to the ionization free path $l_I = \varepsilon_I/E$, one can write the distribution function of the high-energy particles that are few in number

$$f(\varepsilon) \sim \exp\left(-\frac{l(\varepsilon)}{l_c}\right) = \exp\left(-\frac{\varepsilon}{l_c eE}\right). \tag{27}$$

Taking into account Eqs. (22), (23) and (25) as well as the fact that $W_I \neq 0$ only for $\varepsilon \geq \varepsilon_I$, one concludes immediately that in the low field limit

$$\alpha(E) \sim \exp\left(-\frac{\varepsilon_I}{l_c eE}\right), \qquad g(E) \sim \exp\left(-\frac{\varepsilon_I}{l_c eE}\right). \tag{28}$$

The dependence (28) is often used for the interpretation of the experimental data in narrow gap semiconductors in the low field region when the ionization rate is low.

More general and much more complicated numerical Monte Carlo simulations that can, in principle, describe the impact ionization process throughout a wide field region, were also used for the study of impact ionization in narrow gap materials [41,29,61,83]. We will discuss the results obtained using this method in more detail in the material-specific sections below.

3. Mercury–cadmium telluride

3.1. Band spectrum and material parameters

The band spectrum of $Hg_{1-x}Cd_xTe$ (see Fig. 4) is usually described by the Kane band model [78]. It includes four bands: the conductivity band E, the degenerate valence band that consists of the light hole and heavy hole bands (B and A, respectively), and the spin-split band C. As the spin-orbital splitting Δ, i.e., the energy interval between the extrema of the valence band B and spin-split band C, is large, $\Delta \approx 1$ eV, the three band approximation of the Kane model works well for the description of the carrier dispersion laws in the narrow gap alloys when $\varepsilon_g \ll \Delta$. The Hamiltonian of the model under this approximation can be found in Refs. [55,19,53], and we will
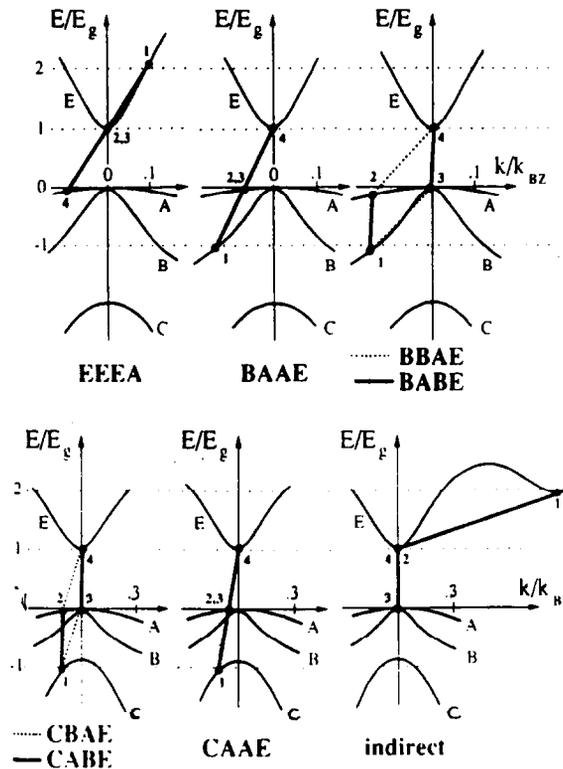

Fig. 4. The Auger transitions in the band structure of $Hg_{1-x}Cd_xTe$ [83].

not reproduce it here. Generally, the corresponding band spectrum is anisotropic, but a small warping of the equal energy surfaces is often neglected. The dispersion laws of the electrons and light holes coincide in this approximation and are given by the equation

$$\frac{\hbar^2 k^2}{2m_e} = \varepsilon\left(1 + \frac{\varepsilon}{\varepsilon_g}\right).$$ (29)

The effective mass of electrons, m_e, and that of light holes, m_l, at the bottom of the bands are the same and can be expressed as

$$\frac{1}{m_e} = \frac{2P^2}{\hbar^2 \varepsilon_g} + \frac{1}{m_0} = \frac{1}{m_0}\left(\frac{2m_0 P^2}{\hbar^2 \varepsilon_g} + 1\right),$$ (30)

where m_0 is the free-electron mass, P is the Kane matrix element, $2m_0 P^2/\hbar^2 = 18$ eV [122], which is practically composition and temperature independent for $Hg_{1-x}Cd_xTe$. On the contrary, ε_g is a function of x and T, and a number of phenomenological expressions for $\varepsilon_g(x, T)$ can be found in the literature. We reproduce one of them here that was presented in Ref. [33] and is valid for $0 < x < 0.6$ and $4.2 < T < 300$ K

$$\varepsilon_g(x, T) = -0.302 + 1.93x + 5.35 \times 10^{-4} T(1 - 2x) - 0.810x^2 + 0.832x^3.$$ (31)

Here T is in degrees Kelvin and ε_g is in eV.

According to Eqs. (30) and (31), m_e can vary over a wide range as the alloy composition is varied. The heavy hole mass M_h is not sensitive to the composition and equals $(0.4-0.6) \times m_0$ [47, 99, 122].

The value of the high frequency dielectric constant κ_∞ in $Hg_{1-x}Cd_xTe$ equals 9.8–14 [46, 53].

3.2. Auger recombination

3.2.1. Theory

The different possible Auger transitions in $Hg_{1-x}Cd_xTe$ and the alloy composition dependence of the corresponding ionization threshold energies are presented in Figs. 4 and 5 [83]. The electron states are denoted 1 to 4 instead of 1, 2, 1' and 2' but we hope that this will not confuse the reader. One can see from these figures that only the transitions shown in the upper row in Fig. 4 can take place in narrow gap alloys with $x \approx 0.2-0.3$ when $\varepsilon_g \ll \Delta$, the spin-orbital splitting. The first transition labelled EEEA in the figure is an eeh process, and the other two are ehh transitions. The threshold energies can be found in Ref. [83] from the full tight-binding band structure calculations using a set of 14 orbitals. So the results are valid over the full composition range. The anisotropy of the spectrum has also been taken into account in this approach, which is not large and is usually neglected. Of course, for the narrow gap compositions the results are close to those that have been found earlier with the help of the three band approximation of the Kane model (see Eq. (19)). The activation energy ε_g^{ehh} in Eq. (19) corresponds to the BAAE transition, and the activation energies for the other processes from the upper row in Fig. 4 equal ε_a^{eeh} because the electron and light hole bands become mirror-symmetric for $\varepsilon_g \ll \Delta$. As a consequence, the rate of the BAAE transitions is much higher than that of the other ehh channel because of smaller activation energy and larger
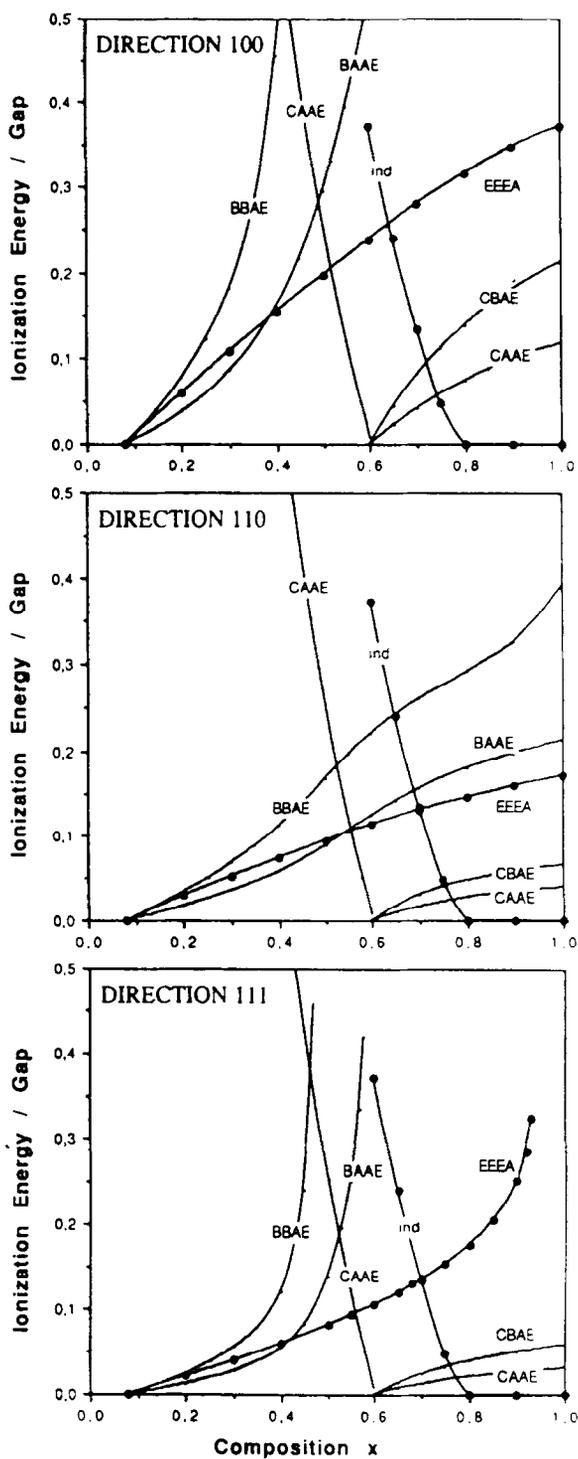
Fig. 5. Ionization energy for different Auger processes (see Fig. 4) as a function of HgTe content for different momentum directions of the ionizing carrier. The ionization energies are calculated from the minimum ionization energy ($\varepsilon_{1\,\mathrm{min}} = \varepsilon_{\mathrm{g}}$) [83].

density of states in the heavy hole band. One cannot neglect, however, the rate corresponding to the eeh channel using similar arguments because $R_{eeh} \sim n^2 p$ whereas $R_{ehh} \sim np^2$ (see Section 2.1), and the relative importance of eeh and ehh transitions depends on the temperature and carrier concentrations (see Eq. (34)). So one has to consider two Auger transition channels, one of eeh type (EEEA) and the other of ehh type (BAAE).

A considerable number of articles have been devoted to the calculation of the Auger rate in $Hg_{1-x}Cd_xTe$ [54–57, 60, 62, 35, 34, 15, 49, 44]. More detailed theoretical calculations can be found in the series of papers by Gelmont [54–57, 60].

In [54, 55] the carrier band spectrum in $Hg_{1-x}Cd_xTe$ was described by the three-band Kane model that approximates the material's band dispersion law with a high precision in the narrow gap material. The eeh-transitions that were considered are more important in n-type material. Two electrons and a heavy hole take part in this process (see Fig. 1). The specific feature of the Kane spectrum is that the interband overlap integral of the Bloch amplitudes of the carrier wave functions equals zero at the Auger transition threshold, and this fact was first taken into account simultaneously by Gelmont [54, 55] and by Gerhardts et al. [62]. In the simplified approach to the Auger rate calculation, when the Bloch structure of the carrier wave functions is neglected [16, 35, 34], the interband overlap integral is assumed to be a non-zero constant at the threshold. When the correct form of the overlap integral is incorporated into the calculations, the temperature dependence of the calculated transition rate differs from that obtained when the precise structure of the wave functions is not taken into account. Furthermore, if the electrons are degenerate, the correct concentration dependence of the rate [55, 62] also turned out different in comparison with the simplified approach.

If electrons and holes are non-degenerate and the temperature T is much less than ε_g, the following expression for the Auger transition rate, either recombination or ionization, in thermo-dynamical equilibrium has been obtained [55] for the eeh process which is more important in n-type material:

$$R_e = A_e n_i^2 n ,$$

$$A_e = 3 \sqrt{\frac{2}{\pi}} \frac{m_e e^4}{\kappa^2 \hbar^3 N_c^* N_v^*} \left(\frac{T}{\varepsilon_g}\right)^{5/2} \exp\left(-2 \frac{m_e \varepsilon_g}{M_h T}\right) , \tag{32}$$

where n is the actual electron concentration, $n_i = \sqrt{N_c^* N_v^*} \exp(-\varepsilon_g/2T)$ is the electron concentration in the intrinsic material, m_e and M_h are the electron and heavy hole masses, respectively, N_c^* and N_v^* are the effective numbers of states in the bands (see Eq. (14)), and κ is the value of the dielectric constant which corresponds to the frequency of the transition at the threshold of the process. If the gap width exceeds the optical phonon energy which is the case for technologically important alloys with $x = 0.2$ and 0.3, then one can substitute the high-frequency dielectric constant κ_∞ for κ in Eq. (32). We remind the reader that $np = n_i^2$ at equilibrium and so Eq. (32) has essentially the same form as Eq. (17).

The effect of the warping of the heavy hole band on eeh recombination velocity has been studied in Ref. [55] and it turned out to be small.

Auger transitions in the p-type Kane semiconductor were considered in Ref. [57] under similar assumptions. In this case, the ehh transition channel is important (see Fig. 2). For the ehh
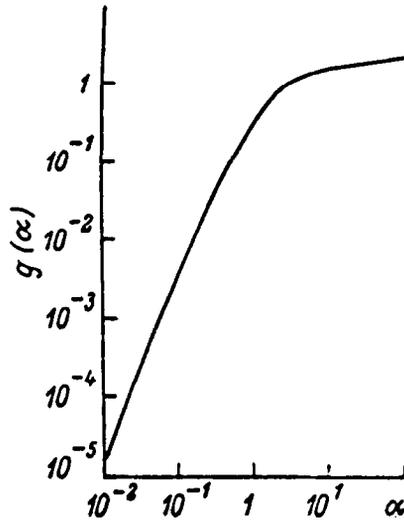
Fig. 6. Plot of $g(\alpha)$ [57].

mechanism there is one electron and two heavy holes in the initial state, and one of the holes jumps into the light hole band after the transition. The expression for the ehh transition rate at thermodynamical equilibrium (for either recombination or impact generation) is as follows:

$$R_h = A_h n_i^2 p \,,$$
(33)

$$A_h = \frac{18 M_h e^4}{\pi \kappa^2 \hbar^3 N_c^* N_v^*} \left(\frac{T}{\varepsilon_g}\right)^{7/2} g\left(\frac{m_e \varepsilon_g}{M_h T}\right) \exp\left(-\frac{m_e \varepsilon_g}{M_h T}\right).$$

This expression is valid for non-degenerate electron and hole distributions at temperatures much less than ε_g. In Eq. (33), p is the hole concentration, and the function $g(\alpha)$, $\alpha = m_e \varepsilon_g/(M_h T)$, is expressed through a one-dimensional integral. The results of numerical calculations of $g(\alpha)$ are presented in Fig. 6 [57]. In the limiting cases g reduces to

$$g(\alpha \gg 1) = \frac{3\sqrt{\pi}}{2} \,;$$

$$g(\alpha \ll 1) = \frac{3\pi^2}{16} \alpha^{5/2}$$

(we have corrected a misprint in Ref. [57] where $\alpha^{5/2}$ stood in the denominator).

One can see from the expressions for A_e and A_h that the activation energy for the ehh transitions is two times less than that for eeh, in agreement with Eq. (19).

Using Eqs. (32) and (33), one can easily find the ratio of the ehh rate to the eeh one:

$$\frac{R_h}{R_e} = 3 \sqrt{\frac{2}{\pi}} \frac{p}{n} \frac{e^\alpha g(\alpha)}{\alpha}, \quad \alpha = \frac{m_e \varepsilon_g}{M_h T} = \frac{\varepsilon_a^{ehh}}{T}.$$
(34)

It is evident that small α values (i.e. $T \gg \varepsilon_a^{ehh} = (m_e/M_h)\varepsilon_g$) are favourable for eeh transitions, whereas ehh ones may be important at lower temperatures when α becomes large.

Both Eqs. (32) and (33) were obtained with the help of the method of Beattie and Landsberg.

The quantity that is usually measured in experiments is the lifetime of the non-equilibrium carriers. To connect it with the calculated Auger coefficients, let us consider the carrier balance equations taking into account the recombination via eeh and ehh channels as well as the reverse process, i.e. impact ionization:

$$\frac{\partial n}{\partial t} = \frac{\partial p}{\partial t} = (A_e n + A_h p)(n_i^2 - np) . \tag{35}$$

Then, for the small-signal Auger lifetime, when densities of the excess carriers are much less than the equilibrium concentrations, one obtains

$$\frac{1}{\tau} = (n_0^2 + n_i^2)A_e + (p_0^2 + n_i^2)A_h , \tag{36}$$

where n_0 and p_0 are the equilibrium carrier densities.

Th typical shape of the temperature and extrinsic carrier concentration dependence of the lifetimes in n- and p-type material are shown in Fig. 7 [96]. In this article calculations according to Gelmont's formulae were performed for $Hg_{1-x}Zn_xTe$, the narrow gap semiconductor with the Kane spectrum and with the material parameters similar to those of $Hg_{1-x}Cd_xTe$. The lifetimes calculated using the results of Ref. [35] when the interband overlap integral is treated as a constant
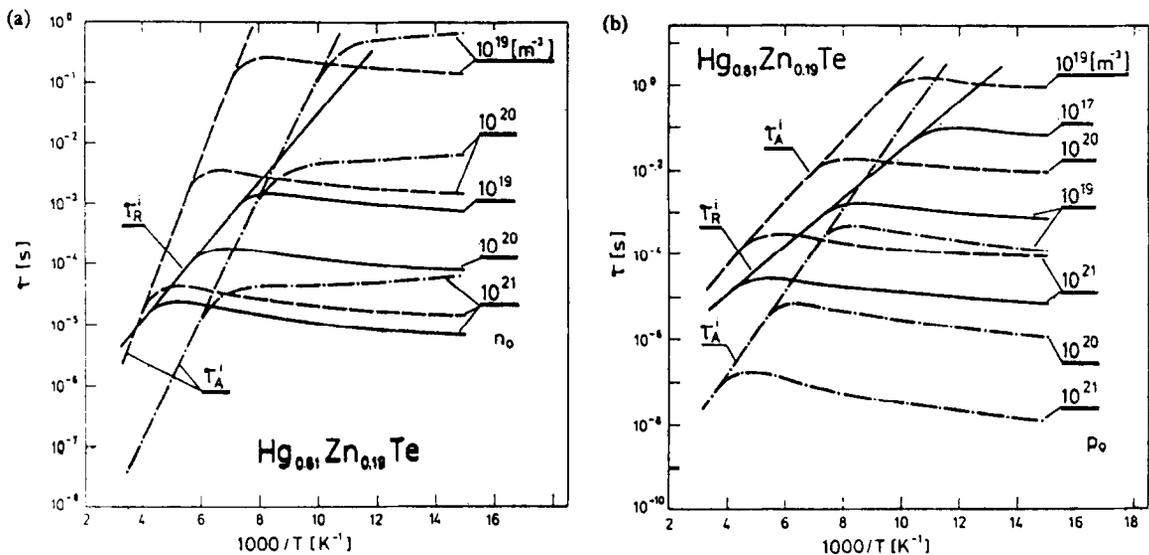

Fig. 7. Temperature dependence of the calculated carrier lifetime in (a) n-type and (b) p-type $Hg_{0.81}Zn_{0.19}Te$ [96]. τ_R, the radiative lifetime; τ_A, the Auger lifetime; dashed line; Casselman–Petersen theory; dashed–dotted line, Gelmont theory.

are also shown in the same figure. One can see that the latter approximation gives incorrect temperature dependence of both electron and hole lifetimes. Of course, the concentration dependence of the lifetimes remains the same in both approaches because it is determined entirely by the classical carrier statistics.

The situation changes when the electrons become degenerate. In Ref. [56] the Auger rate was calculated for this case under the assumption that the Fermi energy of the electrons was small as compared to ε_g and that the holes were non-degenerate. The main Auger process is eeh here.

The equation of the electron concentration balance in this case is as follows:

$$\frac{\partial n}{\partial t} = A_e N_c^* n \mathscr{F}_{3/2}(\zeta/T) \left[p_0 \exp\left(\frac{\zeta_0 - \zeta}{T}\right) - p \right],$$

$$n = N_c^* \mathscr{F}_{1/2}(\zeta/T) ,$$

$$(37)$$

where

$$\mathscr{F}_\nu(z) = \frac{1}{\Gamma(\nu + 1)} \int_0^\infty dx \frac{x^\nu}{1 + \exp(x - z)}$$

is the Fermi integral, $\Gamma(\nu)$ is the Γ-function, ζ_0 is the equilibrium value of the carrier chemical potential, and A_e is the Auger coefficient for the eeh channel (see Eq. (32)).

Expanding Eq. (37) about small deviations of the carrier concentration from its stationary value, one can find in the linear approximation the small-signal lifetime of the electrons at an arbitrary excitation level and degree of degeneracy. The following expression [56] corresponds to highly degenerate electrons $(T \ll \zeta_e)$ and low excitation $(n - n_0 \ll n_0)$:

$$\frac{1}{\tau} = \frac{8\hbar^5 (3\pi^2 n_0)^{5/3} A_c N_c^*}{15 \sqrt{\pi} (2m_e T)^{5/2}} \left[n_0 + \frac{\hbar^2 p_0 (3\pi^2 n_0)^{2/3}}{3m_e T} \right].$$

$$(38)$$

At high excitation levels when $n = p$ and electrons are degenerate (but the condition $\varepsilon_F \ll \varepsilon_g$ still holds), the lifetime is given by the following expression

$$\frac{1}{\tau} = \frac{88\hbar^5 (3\pi^2)^{5/3} A_e N_c^* n^{8/3}}{45 \sqrt{\pi} (2m_e T)^{5/2}} .$$

$$(39)$$

It follows from Eq. (39) that $\tau \sim n_0^{-8/3}$ for the degenerate n-type semiconductor whereas the calculations with a constant value of the interband overlap integral give $\tau \sim n_0^{-2}$ [34]. The power $(-\frac{8}{3})$ in the concentration dependence of τ was found simultaneously in Ref. [62] but it was given there without derivation.

The region of high electron concentration in n-type material when the Fermi energy of the electrons is comparable to ε_g was investigated numerically in Ref. [35,34]. It was already mentioned above that there is no suitable analytical method for these conditions. As the carrier energy is high, the transitions are no longer concentrated near the threshold but they take place from a wide region of the momentum space with dimensions that are comparable to the k_2' value at the threshold. As a consequence, the precise forms of the overlap integrals are not as important here as in the low-temperature near-threshold case, because the integrals are averaged now over a wide

region in k-space. Hence one can expect that the use of the simple constant approximation for them in Refs. [35, 34] probably did not influence significantly the concentration dependence of the lifetime. The numerical calculations showed that the electron lifetime due to the eeh process in a degenerate electron gas is proportional to n^{-a}, where $a = 0.7$–1.0 depending upon the relations between T, ζ_e and ε_g.

Another numerical calculation of the Auger transitions in $Hg_{1-x}Cd_xTe$ was carried out in Ref. [15]. In contrast to the approach of Casselman and Petersen, the Kane band model was used here for calculation of the overlap integrals as in the theory of Gelmont. Taking carrier degeneracy into account, the Auger recombination and ionization rates for both eeh and ehh processes were calculated in $Hg_{0.8}Cd_{0.2}Te$ but for comparatively low carrier concentration n up to $10^{15}\,cm^{-3}$ so that the Fermi energy remains much less than ε_g. The results are presented in Figs. 8–10 [15]. In Fig. 8, the temperature dependence of the Auger coefficients is shown. The coefficients $A_{e,h}$ and $B_{e,h}$ for recombination and ionization, respectively, are defined through the transition rates by the usual expressions
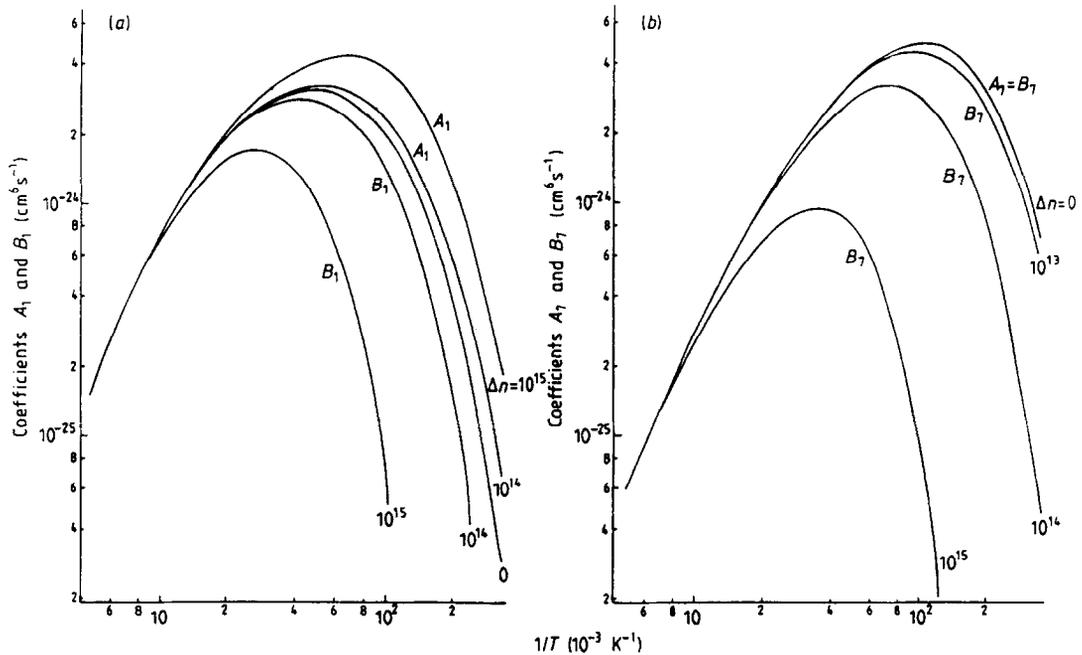
$$R_e = A_e n^2 p\,, \qquad R_h = A_h n p^2 \tag{40}$$

Fig. 8. Calculated Auger recombination coefficients A and impact ionization coefficients B as functions of temperature T for various excess carrier densities in $Hg_{1-x}Cd_xTe$ with $x = 0.2$ and $N_d = 10^{14}\,cm^{-3}$ [15]. (a) The coefficients for the eeh transition (Auger transition 1), where for the curve with $\Delta n = 0$, $A_1 = B_1$. (b) The coefficients for the ehh transition (Auger transition 7). Since A_7 is only weakly dependent on Δn except at the lowest temperatures as can be seen from Fig. 9, the graphs for A_7 with $\Delta n > 0$ are not shown.
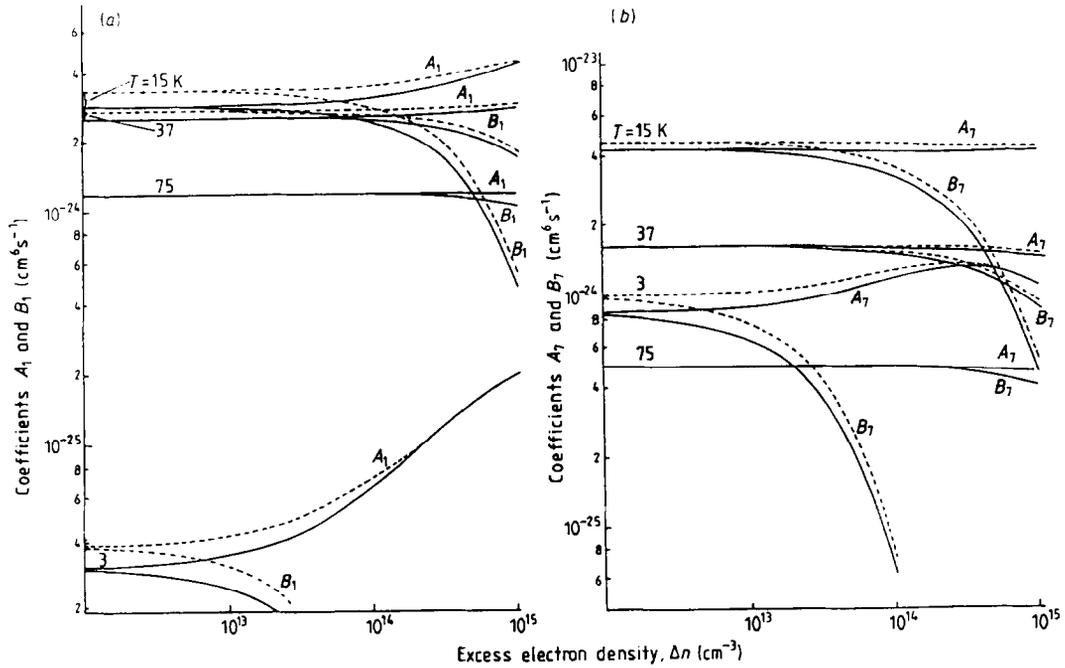
Fig. 9. Calculated recombination coefficients A and impact ionization coefficients B at various temperatures as functions of excess electron density for n-type samples of $Hg_{1-x}Cd_xTe$ with $x = 0.2$. The coefficients for eeh transitions, A_1 and B_1, are shown in (a) and those for ehh transition, A_7 and B_7, in (b). Full curves, $N_d = 10^{-14}\,cm^{-3}$; broken curves, $N_d = 10^{15}\,cm^{-3}$ [15].

for recombination and

$$I_e = B_e n p_0 n_0 , \qquad I_h = B_h p_1 n_0 p_0^2 / p_{10} \qquad (41)$$

for ionization. Here subscript e denotes the eeh process and h the eeh one, p_1 is the concentration of the light holes that are the ionizing particles in the ehh process, and subscript 0 stands for the equilibrium values of the concentrations. Of course, in the case of degenerate statistics, the Auger coefficients in Eqs. (40) and (41) depend upon carrier concentrations as shown in Fig. 9.

In these lifetime calculations, the influence of the 300 K background radiation that may fall on the sample was taken into account [15]. It produces an additional density of non-equilibrium electron–hole pairs and hence influences the mean lifetime. It is clear from Fig. 10 that even a small flux of the 300 K radiation may change the low-temperature carrier lifetime noticeably. The experimental data from Ref. [62] that are also shown in the figure agree well with the calculated curves. It is worth noting, however, that in the original paper [62], the same data were explained by the Auger recombination without taking the 300 K background into account and the agreement with their calculations was also good.

3.2.2. Experiment

We will turn now to the experimental evidence of the Auger recombination processes in $Hg_{1-x}Cd_xTe$. All data correspond to the alloy with $x \approx 0.2$, which has a smaller gap width in
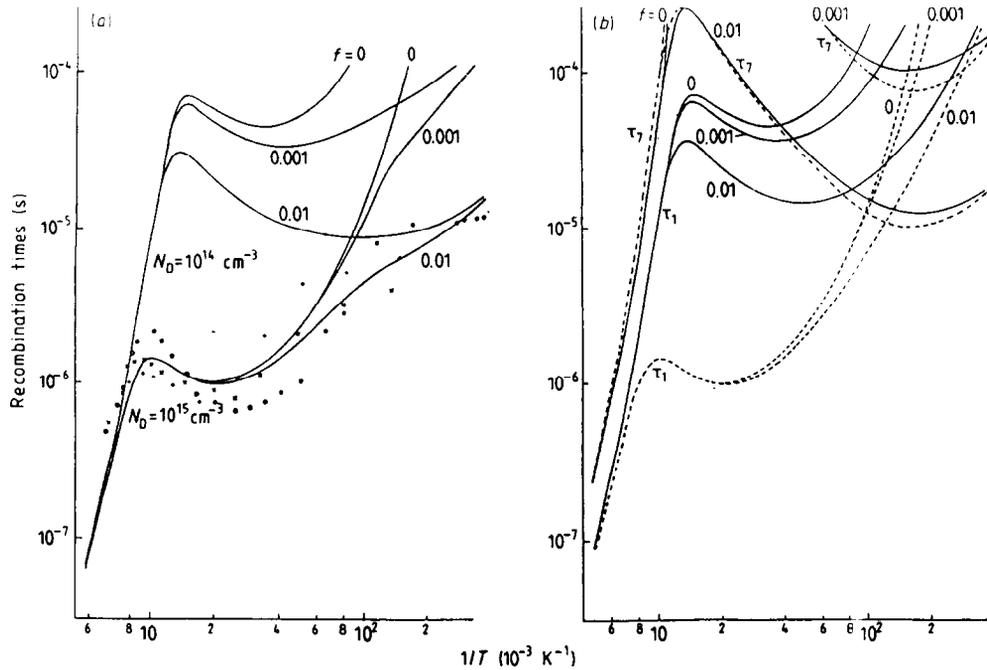
Fig. 10. Calculated Auger recombination times in n-type $Hg_{1-x}Cd_xTe$, $x = 0.20$, as functions of temperature for various fractions, f of 300 K background radiation. (a) The combined recombination time for eeh and ehh transitions and experimental points [62] are also plotted for different extrinsic electron density n_{ex}: (O) $n_{ex} = 4 \times 10^{14} cm^{-3}$; (×) $n_{ex} = 1.3 \times 10^{15} cm^{-3}$; (+) $n_{ex} = 1.7 \times 10^{15} cm^{-3}$. (b) The recombination times for eeh and ehh transitions, τ_1 and τ_7, respectively, shown separately: full curves: $N_d = 10^{14} cm^{-3}$; broken curves: $N_d = 10^{15} cm^{-3}$ [15].

comparison with the other popular compositions, and hence is favourable for Auger recombination (see Section 2.1).

The paper [62] cited above appears to be the only one where $\tau(T)$ dependence was explained entirely by Auger recombination over the wide temperature interval $2 < T < 200$ K that includes the liquid helium temperature region (see Fig. 11). Their measurements were performed using samples with a rather low extrinsic electron concentration 4×10^{14} to 1.7×10^{15} cm^{-3}. They also carried out theoretical calculations similar to those of Gelmont (see the preceding section); the corresponding results are also shown in Fig. 11.

A narrower temperature interval $80 < T < 160$ K was investigated in Ref. [123]. This interval covered, however, both regions of the intrinsic and extrinsic conductivity. The observed temperature dependence of the lifetime coincided with that calculated according to Ref. [16] for all the eight samples investigated. The measured $\tau(n_0)$ dependence in the interval of the extrinsic electron density $n_0 = 3 \times 10^{14}$ to 6×10^{15} cm^{-3} was typical for Auger recombination in the case of non-degenerate statistics: $\tau \sim n_0^{-2}$.

In [31, 5] the recombination in n-$Hg_{1-x}Cd_xTe$ with x around 0.2 and $n_0 = 2 \times 10^{13}$ cm^{-3} was investigated. The temperature was low, $4.2 < T < 13$ K, so the concentration of intrinsic carriers was negligible, and the electron density did not depend upon T, which was evident from the Hall effect measurements. The carrier lifetime increased rapidly as the temperature was decreased:
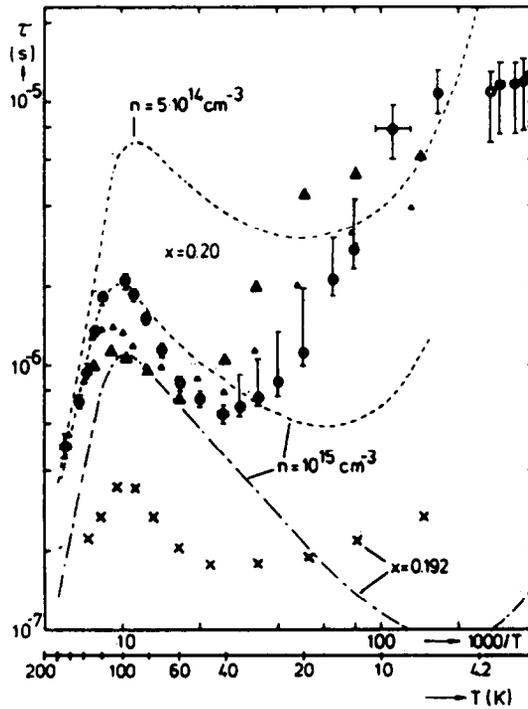
Fig. 11. Experimental lifetime data versus temperature in different n-$Hg_{1-x}Cd_xTe$ samples (closed triangles: $x = 0.20$, the extrinsic electron concentration $n_{ex} = 1.3 \times 10^{15}$ cm^{-3}; open triangles: $x = 0.20$, $n_{ex} = 1.7 \times 10^{15}$ cm^{-3}; crosses: $x = 0.192$, $n_{ex} = 7 \times 10^{14}$ cm^{-3}; dashed and dashed-dotted lines: theoretical values for comparison [62].

$\tau \sim T^{-3.3}$. The lifetime value approached 1 μs at $T = 4.2$ K. It appears to be the largest lifetime value observed in $Hg_{1-x}Cd_xTe$ with $x = 0.2$. The rapid low temperature increase of a lifetime was attributed to the Auger recombination, for which the calculations predict a similar behaviour (see Fig. 10, the curves corresponding to the absence of the background radiation).

In a number of articles where n-type samples were studied [13, 10, 103, 3], as well as the p-type ones [125, 111], the Auger recombination was used to explain a sharp decrease of the lifetime when the temperature was raised in the region of intrinsic conductivity (whereas it was assumed that at lower temperatures the lifetime was limited by the carrier recombination through impurity states, see Section 3.5). This interpretation was sometimes supported by the observation of the concentration dependence of the lifetime $\tau(p_0) \sim p_0^2$ [3], where it has been found over the equilibrium hole concentration interval $1.2 \times 10^{16} \le p_0 \le 5.5 \times 10^{17}$ cm^{-3}.

In many experimental papers the only evidence for the presence of the Auger transitions was that the value and the temperature dependence of the lifetime were close to those calculated for the Auger recombination process. It is worth noting, however, that, generally, one cannot unambiguously identify the recombination mechanism using the temperature dependence of the carrier lifetime only. For example, in Ref. [13] the measured $\tau(T)$ dependences which appeared quite similar to those obtained in Ref. [62] were explained invoking Shockley–Read recombination in the region of extrinsic conductivity (see Fig. 12). Only a combined investigation can give solid
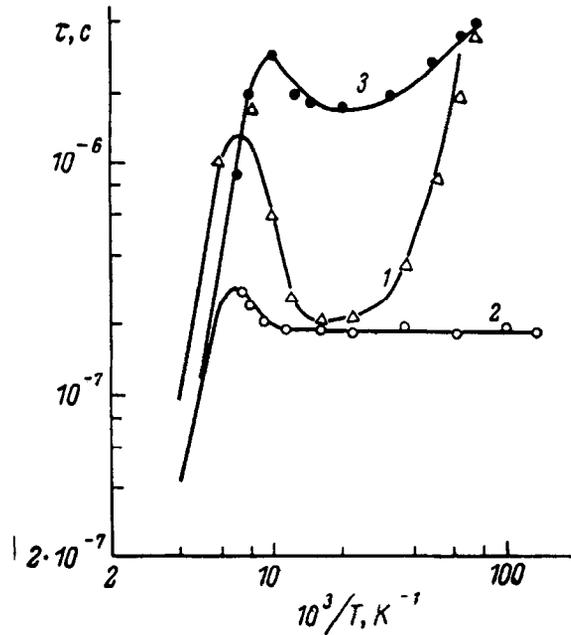
Fig. 12. Experimental temperature dependence of the lifetime in n-$Hg_{1-x}Cd_xTe$ [13]. (1) $x = 0.22, n = 2 \times 10^{15} cm^{-3}$; (2) $x = 0.21, n = 0.89 \times 10^{15} cm^{-3}$; (3) $x = 0.21, n = 1.1 \times 10^{15} cm^{-3}$. Lifetime is given in seconds.

evidence for a definite recombination mechanism. For example, in the series of works by Hangleiter [67–69] on Si samples not only was the dependence of the lifetime on T, n_0 and the excess carrier concentration measured in wide intervals of the parameters and found to be typical for Auger recombination, but also the photoluminescence spectra in the spectral region around $2\varepsilon_g$ were studied, which made it possible to observe the radiation of the hot carriers that appeared as a result of the Auger process. Combined investigations of this kind have not yet been carried out in narrow-gap materials. In addition, the results of the early calculations of the Auger rates with a constant value of the interband overlap integral were often used in experimental papers for data fitting instead of the more precise formulae of Gelmont or the results of Gerhardts–Dornhaus–Nimtz and Beattie, which might introduce a considerable error (see Fig. 7).

3.3. Impact ionization

The impact ionization in $Hg_{1-x}Cd_xTe$ attracted considerably less attention than the electron–hole recombination.

As mentioned above, at equilibrium the ionization rate in $Hg_{1-x}Cd_xTe$ is given by Gelmont's formulae (32) and (33) for ionization by electrons and by light holes, respectively. These expressions are valid also in the non-equilibrium conditions if the distribution of the ionizing particles is given by the Boltzmann function with some effective temperature T^* that should be substituted for T in Eqs. (32) and (33) to obtain the corresponding ionization rate. This approach has been used in Ref. [61] for the calculation of the I–V curves in n-$Hg_{1-x}Cd_xTe$ in a strong electric field that

causes interband breakdown. Monte Carlo simulation of the hot electron distribution function in Ref. [61] showed that its high energy tail which contains the ionizing particles is, actually, close to the simple Boltzmann exponential function.

Another Monte Carlo study of the impact ionization in $Hg_{1-x}Cd_xTe$ was performed in Ref. [83]. The calculated field dependence of the ionization coefficient followed Shockley's formula (see Eq. (28)). The main attention in Ref. [83] was concentrated, however, on the compositions with low-HgTe content and hence with wide gap (of the order of 1 eV), so we will not consider the results obtained there in more detail.

Experimental study of the impact ionization velocity in the narrow gap $Hg_{1-x}Cd_xTe$ has been carried out in a series of papers by Bogdanov and co-workers [22–25]. The n-type specimens with $x \approx 0.20$ were used for the measurements with electron concentration $n_{77K} \approx 4 \times 10^{14}\,cm^{-3}$ and electron mobility around $1.6 \times 10^4\,cm^2/Vs$. The ionization velocity has been measured at $T = 4.2$ and 77 K as a function of the applied electric field E in the interval 150 to 300 V/cm. The field dependence of the ionization coefficient agreed well with Shockley's formula

$$g(E) = g_0 \exp(aE),$$

where

$$g_0[4.2\,K] = 1 \times 10^5\,s^{-1};\qquad a^{-1}[4.2\,K] = 25\,V/cm;$$

$$g_0[77\,K] = 5.6 \times 10^5\,s^{-1};\qquad a^{-1}[77\,K] = 55\,V/cm.$$

The ionization coefficient decreases when the temperature is raised because the energy gap increases with the temperature (see Eq. (31)). The $g(E)$ dependence is illustrated in Fig. 13 [23].

At higher electric field, the ionization rate rises and Shockley's exponential field dependence for g is no longer valid. The actual $g(E)$ increase becomes slower (see Fig. 14 [46]). The authors of Ref. [46] gave no indication to what temperature their data correspond to but it is likely that they observed the impact ionization at 77 K because other measurements they included in Fig. 14 for comparison were carried out at liquid nitrogen temperature. Some inconsistency in the results obtained by different groups that is evident in Fig. 14 is probably connected with the errors in the determination of the alloy composition.

The magnetic field effect on the impact ionization velocity in n-$Hg_{1-x}Cd_xTe$ was studied both experimentally and theoretically in Refs. [24,25]. As the magnetic field was raised, a non-monotonic variation of the electric field that causes the breakdown was observed, which was explained by the effect of the Hall electric field on the electron heating and ionization (the so-called transverse breakdown).

3.4. Radiative recombination

As the gap width is increased, the relative importance of the Auger recombination decreases, and in $Hg_{1-x}Cd_xTe$ with $x \approx 0.3$ another intrinsic interband recombination process becomes more important, namely radiative recombination. In full analogy with what is reported in standard textbooks in the case of wide gap semiconductors (see, for example, [27,115]), the radiative recombination rate in narrow gap materials can be easily expressed in terms of the absorption coefficient, $\alpha(\omega)$. The latter can be determined experimentally [21,39] or calculated [7,89]. Using
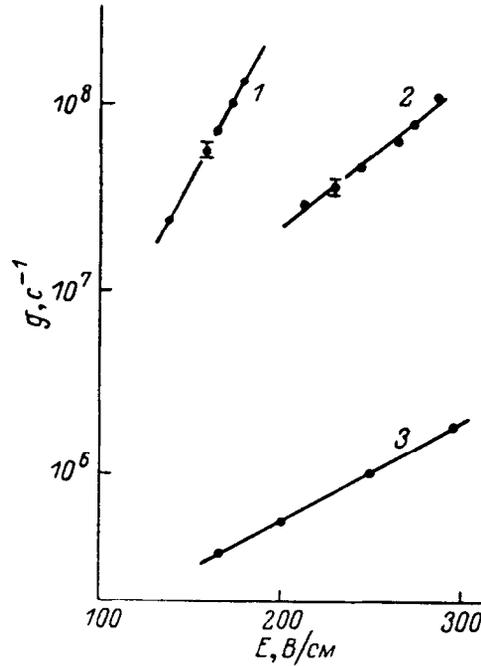
Fig. 13. Electric field dependence of the electron impact ionization velocity in n-$Hg_{1-x}Cd_xTe$ with $x = 0.20$ (1) at 4.2 K and (2) at 77 K [22, 23] and in $Hg_{1-x}Cd_xTe$ with $x = 0.205$ (3) at 77 K [97]. g is measured in s^{-1}, E in V/cm.

the experimental data obtained by Blue [21], the radiative carrier lifetimes in $Hg_{1-x}Cd_xTe$ were determined in Ref. [104]. More often the lifetime was calculated using theoretical values of the absorption coefficient [32, 111]. In these papers the standard $\alpha(\omega)$ dependence for a direct bandgap semiconductor with two parabolic bands was used but more refined calculations for $Hg_{1-x}Cd_xTe$ where its specific band structure was taken into account [7] gave a similar result [111].

The radiative lifetime τ_r is given by the following expression [111]:

$$\tau_r = \frac{\delta n}{R_r(n, p)} = \frac{\delta n \, n_i^2}{G_r^0 np} = \frac{n_i^2}{G_r^0(n_0 + p_0 + \delta n)}, \tag{42}$$

where n and p are the actual carrier densities, n_i is the intrinsic electron concentration, n_0 and p_0 are the equilibrium carrier densities, $\delta n = n - n_0 = p - p_0$ is the concentration of the excess electrons, R_r is the rate of radiative recombination, and G_r^0 is the radiative transition rate at equilibrium [111]

$$G_r^0 = \frac{(k_B T)^3}{\pi^2 c^2 \hbar^3} \int_0^\infty du \frac{\kappa(u)\alpha(u)u^2}{\exp(u) - 1}$$

$$= 5.8 \times 10^{-13} \sqrt{\kappa_\infty} \left(\frac{m_0}{m_e + M_h}\right)^{3/2} \left(1 + \frac{m_0}{m_e}\right)\left(\frac{300}{T}\right)^{3/2}$$

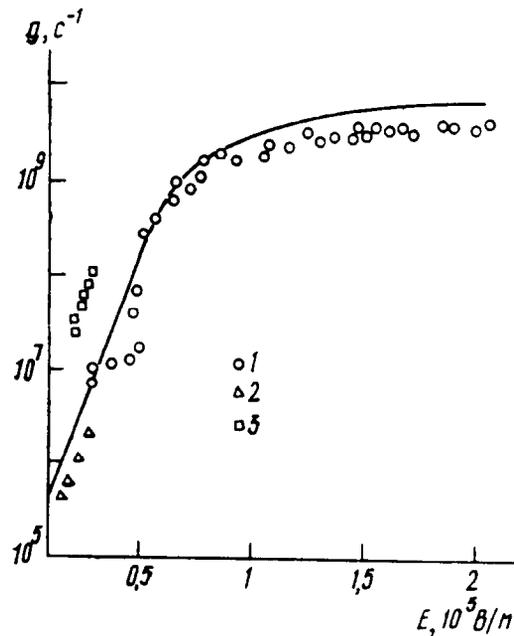$$\times (\varepsilon_g^2 + 3k_B T\varepsilon_g + 3.75(k_B T)^2)n_i^2, \tag{43}$$

Fig. 14. Field dependence of impact ionization velocity in $Hg_{1-x}Cd_xTe$, $x = 0.2$ [46]. (1) Original data of Ref. [46]; (2) data from Ref. [97], $x = 0.205$, $T = 77$ K; (3) data from Refs. [22,23], $x = 0.20$, $T = 77$ K. Solid line, calculation according to the model of Ref. [48]. g is measured in s^{-1}, E in 10^5 V/m.

where α is the absorption coefficient; $u = \hbar\omega/(k_B T)$; ω is the radiation frequency; m_0 is the free-electron mass; κ is the dielectric constant; κ_∞ is the high-frequency dielectric constant; temperature is measured in kelvin, and energies are measured in eV. It was assumed here that $T < \varepsilon_g$. The $\tau(T)$ dependence is shown in Fig. 15 [32].

It is worth noting that the measured radiative lifetime may be noticeably higher than the calculated value due to effects such as the re-absorption of the recombination radiation [70,71], the influence of the background radiation, or the carrier freezeout to impurities [111]. Of course, the two latter factors are not specific for the radiative recombination only as it was discussed in the previous section (see also Ref. [15]).

In experiments, radiative recombination in n- and p-type $Hg_{1-x}Cd_xTe$ with x around 0.3 has been observed in the temperature regions of the intrinsic as well as the extrinsic conductivity but not at the lowest temperatures when the impurity recombination becomes more important [13,6,111,112]. In Fig. 16 [112] the experimental data for n-$Hg_{0.7}Cd_{0.3}Te$ are represented together with the results of calculations of the radiative and Auger transition rates for this material. At $T > 40$ K the typical value of the lifetime and shape of its temperature dependence agree well with those given by the theory of the interband radiative recombination. At lower temperatures the carrier lifetime increases, and two lifetimes can be seen in the recombination kinetics. One of them was attributed to radiative recombination and the other to carrier trapping. Similar $\tau(T)$ dependence found in p-type samples (see Fig. 17) was also explained by radiative recombination together with carrier freezeout to acceptors, and the influence of the background radiation was also taken into account [111].
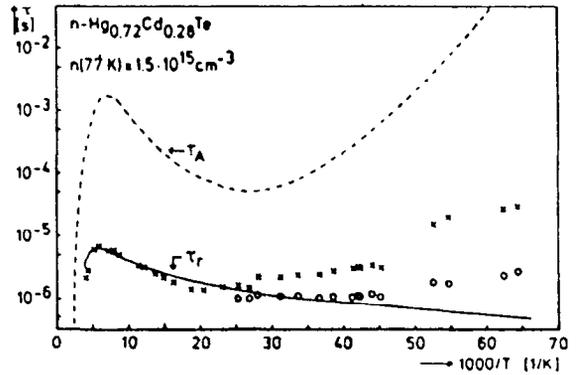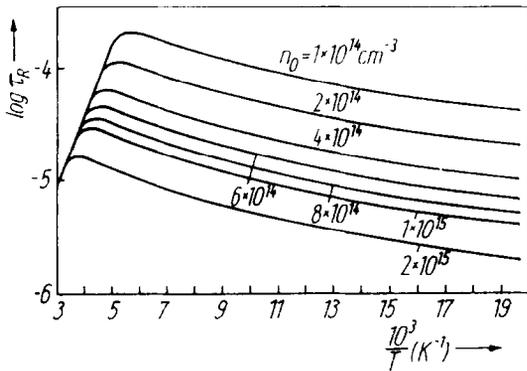
Fig. 15. Calculated radiative lifetime versus temperature for n-Hg$_{1-x}$Cd$_x$Te for different extrinsic carrier concentrations n_0 [32].

Fig. 16. Lifetime versus reciprocal temperature in n-Hg$_{1-x}$Cd$_x$Te [112]. (×) Longer time constant; (○) shorter time constant. Broken line, the Auger theory; solid line, radiative recombination theory.
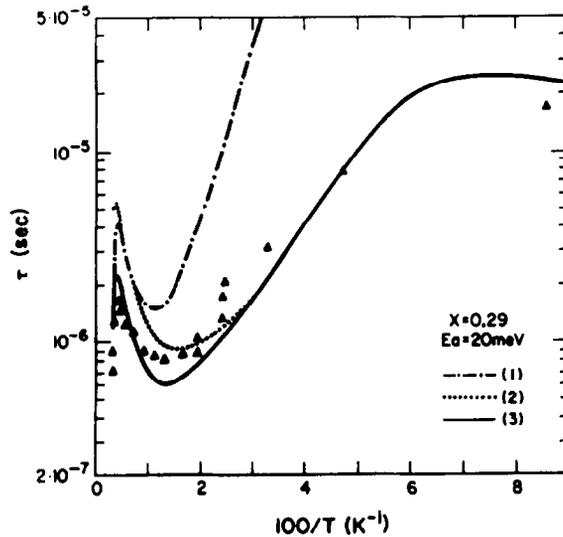

Fig. 17. Triangles, measured lifetime for p-Hg$_{1-x}$Cd$_x$Te samples with $x = 0.29$ and $p_{77\,K} = 7 \times 10^{15}$ cm^{-3}. Calculated lifetime: (1) Auger; (2) radiative; (3) combined [111].

As one can see from the figures, radiative transitions were observed in the samples where carrier lifetime was of the order of several microseconds. But in a series of publications [72, 58, 59, 73, 74], samples with a lifetime smaller by an order of magnitude, were investigated. Nevertheless, it was found [73] that, in these samples at low temperatures $T < 20$ K, the dominant recombination mechanism was radiative recombination. It was, however, no longer the recombination of free

carriers but the radiative recombination of the excitons bound by the impurities. The existence of exciton–impurity complexes in n-$Hg_{1-x}Cd_xTe$ with x close to 0.3 was established using photo-luminescence spectroscopy. The recombination photospectrum consisted of bands, the excitonic nature of which was supported by the specific shape of the magnetic field dependence of their energy [58, 59]. Additional evidence was the temperature dependence of the photoconductivity [73]. Indeed, at 4.2 K the luminescence bands correspond to the minima in the photoconductivity spectrum, but at 15 K these minima are transformed into maxima. The explanation is simple: at lower temperature the excitons created by the external illumination remain stable and do not contribute to the conductivity, whereas at higher temperatures they dissociate into free carriers that manifest themselves in the conduction. The observed luminescence spectra can be caused only by the recombination of the bound excitons because the binding energy of free excitons is too small to explain the observed 10 meV difference between ε_g and the luminescence frequency. Moreover, the structure of the luminescence spectra is sensitive to the impurity concentration in the sample [73].

The connection between the process of radiative recombination of excitons and free carrier lifetime was established with the help of simultaneous measurements of the kinetics of photocon-ductivity and photoluminescence [73]. It was found that a delay exists between the beginning of the exciting light pulse and the appearance of the luminescence, the delay value being equal to 0.2 μs. Photoconductivity measurements have shown that the free carrier lifetime is also equal to 0.2 μs. Hence one can suppose that the free carrier recombination takes place through the formation of the excitons which take approximately 0.2 μs, with their subsequent radiative recombination.

3.5. Shockley–Read recombination

Another important channel for non-equilibrium carrier recombination is the Shockley–Read process that is connected with the radiationless carrier capture into the localized states at impurities and defects. In the simplest case, it is assumed that the trap creates only one energy level in the gap and the electrons and holes are captured by this state in turn.

Statistics of this recombination process and the corresponding temperature and concentration dependence of the lifetime under different observation conditions are discussed in detail in many textbooks (see, for example, [20, 9, 27, 81]). These results are valid in narrow gap materials, too, so we will not reproduce here the well-known expressions.

The key quantities that define the Shockley–Read lifetimes are the cross-sections of the impu-rities, which are usually treated as phenomenological parameters. Generally, the cross-sections can be calculated in the microscopic theory, and that has actually been done for several possible capture mechanisms in wide gap semiconductors [82, 2, 92]. In all these calculations it was assumed that the transition energy was released in the form of numerous phonons. The results obtained in these calculations, however, cannot be directly applied to narrow gap semiconductors. Indeed, the cascade capture mechanism [82, 1] can hardly take place in narrow gap materials because it needs centers with Coulomb potential. But in narrow gap semiconductors the Coulomb binding energies are very small because of the small carrier masses and large dielectric constant values, so levels of the recombination centers appear not to be connected with the Coulomb interaction. The theory of many-phonon capture [2, 92] is not very suitable for narrow bandgap materials because it utilizes the fact that the trap is deep so that its binding energy is much greater than the phonon energy. But in a narrow gap semiconductor where ε_g is small, the trap depth is

often of the order of the optical phonon energy. For example, electron capture by a trap with the emission of only one optical phonon was observed in $Hg_{1-x}Cd_xTe$ [118].

Calculations of the carrier lifetime due to carrier capture into a non-Coulomb trap with the emission of only one phonon have been carried out [42]. It was assumed that the phonon belonged to a local mode, that is, electron energy was transferred to the vibrations of the trap itself. Because electron–phonon coupling is, generally, stronger with local modes, one can suppose this mechanism to be more effective as compared to the transitions with the emission of a polar optical or deformation acoustical phonon. Impurity potential in Ref. [42] was taken in a short-range form as a deep well with a shallow level ε_i. The energy of the level depended upon the center position in the unit cell. This dependence represented interaction with the local phonons. This capture mechanism led to the following expression for the electron lifetime:

$$\frac{1}{\tau} = \frac{8\pi\hbar^3\omega N}{R_0^2 M \kappa_0^2} \sqrt{\frac{2\pi}{m}} \frac{b}{(1+b^2)^3} T^{-3/2} \exp\left(-\frac{\varepsilon_t}{T}\right), \tag{44}$$

where N is the trap concentration; ω is the frequency of the local phonon; M is the reduced mass of the local oscillator (of the order of an atomic mass); R_0 is the value of the center displacement at which the local level of the trap is pushed out from the well, i.e. its energy becomes zero, R_0 being of order of the lattice constant; $\varepsilon_t = \hbar\omega - \varepsilon_i$; $b = \sqrt{\varepsilon_t/\varepsilon_i}$.

At temperatures $T > \frac{2}{3}\varepsilon_t$, the lifetime given by Eq. (44) increases as the temperature is raised. This temperature dependence and the magnitude of the lifetime agree with the observed ones in narrow gap materials [121,90].

Experimental studies of the carrier trapping effect upon the free electron and hole lifetimes have been reported in a large number of papers. The Shockley–Read recombination becomes noticeable, as a rule, in the region of the extrinsic conductivity or in its low-temperature part. The most popular method of determination of the recombination centre parameters is the analysis of the temperature dependence of the lifetime, which makes it possible to find the energy of the impurity levels. A typical temperature dependence of the lifetime is illustrated in Fig. 12 [13]. The lifetimes were measured using samples with $x \approx 0.2$ and electron density $(0.5–2) \times 10^{15}$ cm^{-3} and with $x = 0.3$ and electron concentration $(6–8) \times 10^{13}$ cm^{-3}. Recombination through the impurity level situated 70 meV above the valence band maximum dominates over the temperature interval from 50 to 170 K, whereas the lifetime increase at $T < 50$ K is connected with the hole trapping to the shallow centres with the levels 6 meV above the valence band maximum. In the interval of intrinsic conductivity, Auger recombination plays the main role. Observation of centres with 70 meV levels was reported also in Ref. [8].

In p-type specimens a similar temperature dependence of the lifetime has been observed. Fig. 18 was taken from Ref. [125]. The shape of the $\tau(T)$ curves was explained by recombination via the traps with 30 to 45 meV levels in some of the samples (curves 1, 2, 3, and 6), whereas levels with energy 10 to 15 meV were present in others.

Detailed studies of the deep levels in p-type $Hg_{1-x}Cd_xTe$ were carried out by Polla and Jones with co-workers. Using deep level transient spectroscopy (DLTS) [130] in different modifications as well as the infrared probe technique, they determined the level energies in alloys with different composition. They extracted the lifetime of the non-equilibrium carriers from the photoconductivity decay kinetics and found the lifetime dependence on temperature, equilibrium carrier
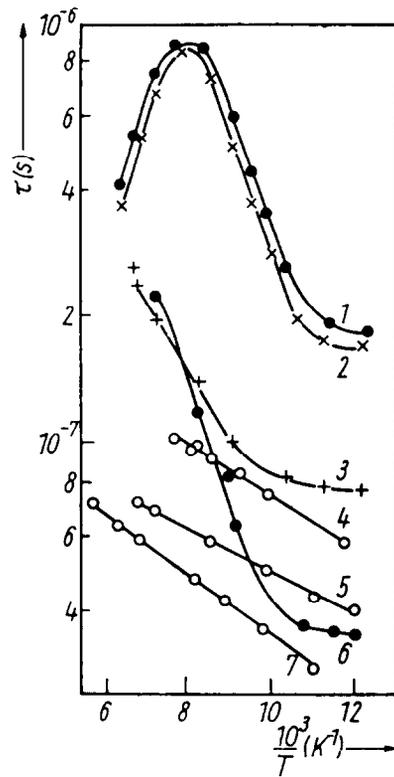
Fig. 18. Temperature dependence of charge carrier lifetime in p-$Hg_{1-x}Cd_xTe$ with composition (1–3) $x = 0.195$ and (4–7) $x = 0.20$ [125]. (1,2) $p_0 = 8 \times 10^{15}\,cm^{-3}$; (4–7) $p_0 = 1.7$–$2.5 \times 10^{15}\,cm^{-3}$. It is not clear what p_0 value corresponds to (3) because there is a controversy between the different data in Ref. [125].

concentration and density of excess electrons. In Figs. 19 and 20 [100] one can see the experimental carrier lifetimes in p-$Hg_{1-x}Cd_xTe$ obtained in n^+–p photodiodes and the results of the calculations according to the Shockley–Read theory. In Fig. 21, taken from the same article, the compositional dependence of the trap level energy is presented. The levels are situated slightly below the midgap.

In another experiment [76] two recombination levels in the gap were found from the temperature dependence of the lifetime. Their energies are approximately $\varepsilon_{v\,max} + \varepsilon_g/2$ and $\varepsilon_{v\,max} + 3\varepsilon_g/4$ (see Fig. 22). Both levels were observed also with the help of DLTS over a wide composition range (Fig. 23). The capture cross-sections of these states were also estimated. For the $\varepsilon_g/2$ level the cross-section for electrons is 10^{-15}–$10^{-16}\,cm^2$ and for holes it equals 10^{-17}–$10^{-18}\,cm^2$, and for the $3\varepsilon_g/4$ level the cross-sections are 10^{-16} and 10^{-17}–$10^{-20}\,cm^2$, respectively.

The electron trap levels in the gap in n-type $Hg_{1-x}Cd_xTe$ with x around 0.3 were also investigated by means of DLTS in metal–insulator–semiconductor structures [40, 36]. The same $\varepsilon_g/2$ and $3\varepsilon_g/4$ (or $2\varepsilon_g/3$) levels were found as in the p-type material. The cross-sections lie in the range 10^{-18}–$10^{-16}\,cm^{-2}$. The role of these levels in carrier recombination has not been clarified, however, in Refs. [40, 36].
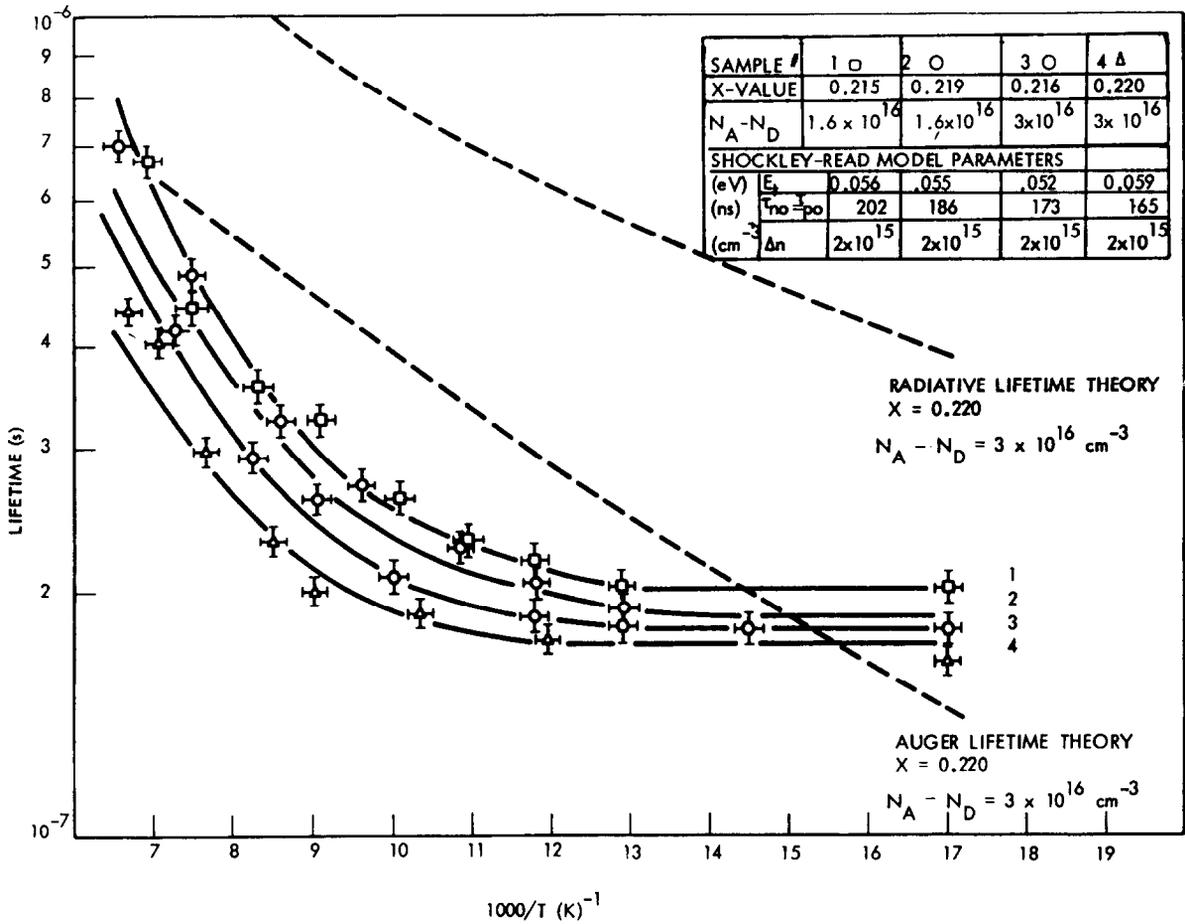
SAMPLE #	1 □	2 O	3 O	4 Δ
X-VALUE	0.215	0.219	0.216	0.220
N_A-N_D	1.6×10^{16}	1.6×10^{16}	3×10^{16}	3×10^{16}
SHOCKLEY-READ MODEL PARAMETERS				
(eV) E_t	0.056	.055	.052	0.059
(ns) $\tau_{no} = \tau_{po}$	202	186	173	165
(cm^{-3}) Δn	2×10^{15}	2×10^{15}	2×10^{15}	2×10^{15}

Fig. 19. Lifetime versus temperature in p-$Hg_{1-x}Cd_xTe$, $x \approx 0.2$, with different acceptor concentrations. The results are explained in terms of a single Shockley–Read recombination center located 55 ± 5 meV above the top of the valence band. Dashed curves show the radiative and Auger lifetime (due to both eeh and ehh processes) [100].

The origin of these levels is not clear. Recent experiments [84] show that the midgap level is probably connected with Hg interstituals. Some other considerations can be found in Refs. [76, 101, 91, 77]. The subject needs further study. The problem is a complicated one, and investigations are in progress.

3.6. Thin films and artificial structures

The carrier recombination processes remain generally the same in thin films that were observed in the bulk. However, the recombination at defects is often enhanced in thin films. First, this is due to the influence of surfaces and interfaces that can be considered as plane defects and may produce numerous recombination levels [129]. Second, thin films often contain a considerable density of
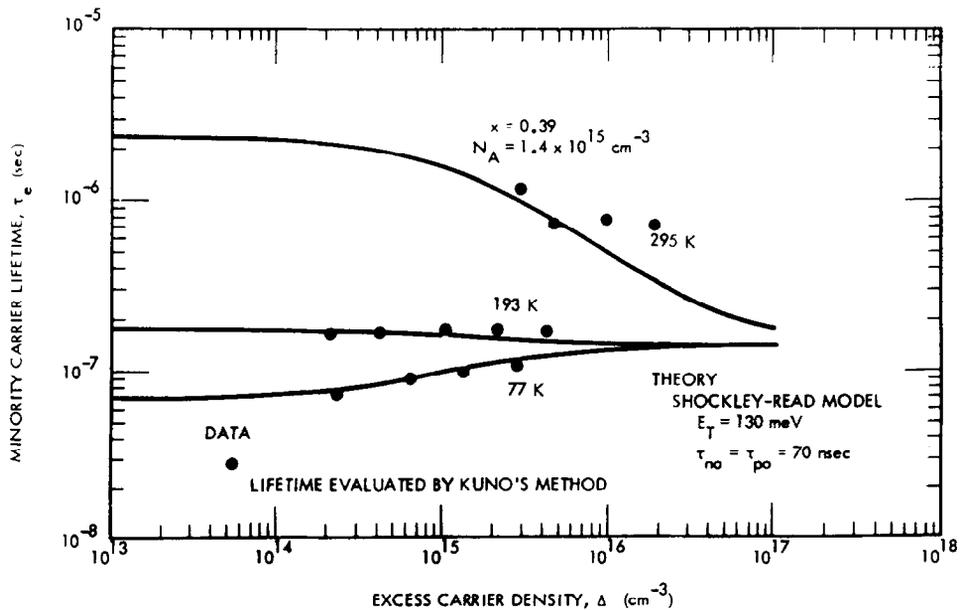
Fig. 20. Dependence of lifetime on the concentration of excess carriers for p-$Hg_{1-x}Cd_xTe$, $x = 0.39$, at 77, 193 and 295 K, with data modelled to Shockley–Read theory [100].

dislocations because of the lattice mismatch between layer and substrate or between different layers [119].

The carrier recombination in thin $Hg_{1-x}Cd_xTe$ films was studied by many authors [134, 10, 64, 63, 3, 116, 95, 12]. Their results show that the carrier lifetimes and their typical temperature and carrier concentration dependence in films with thickness in the μm and sub-μm range are similar to those observed in bulk samples. For example, Figs. 24 and 25 illustrate $\tau(T)$ curves measured in n- and p-type $Hg_{1-x}Cd_xTe$ films grown on GaAs substrates using metalorganic chemical vapour deposition (MOCVD). The data were explained entirely by bulk recombination mechanisms. A similar $\tau(T)$ dependence· was observed in liquid phase epitaxy (LPE) p-$Hg_{1-x}Cd_xTe$, $x = 0.157$ to 0.23 [3] where, in addition, the concentration dependence of the lifetime was measured. Being close to $\tau(p) \sim p^{-2}$ at 77 K, it demonstrated the importance of the Auger recombination in these relatively narrow gap films even at low temperatures. The Shockley–Read levels with energy $\varepsilon_{v\,max} + (0.7–0.8)\varepsilon_g$ were found in both n- and p-$Hg_{1-x}Cd_xTe$ films [116, 3, 134] and, in addition, those with energy $\varepsilon_{v\,max} + (0.25–0.35)\varepsilon_g$ were observed in p-type films [3, 134].

A similar situation occurs also in molecular beam epitaxy (MBE) HgTe/CdTe superlattices [107] where again the magnitude of the lifetime (several hundred nanoseconds) and $\tau(T)$ dependence are close to the values typically observed in a good quality bulk material of comparable band-gap energy (corresponding to the wavelength of approximately 5 μm) and doping level. The experimental data agreed well with the calculated $\tau(T)$ dependence if the entire bulk recombination mechanisms were taken into account. No specific effects of the carrier quantum confinement on the lifetime have been observed in Ref. [107].
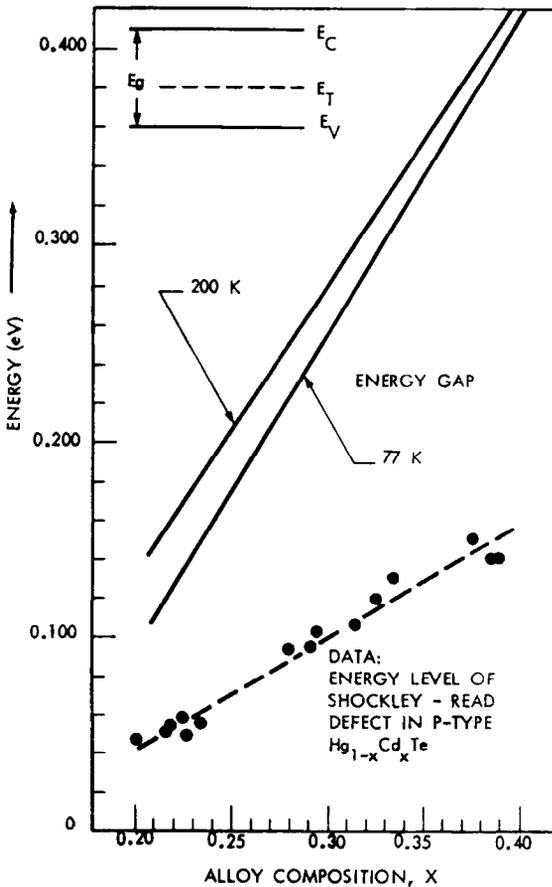
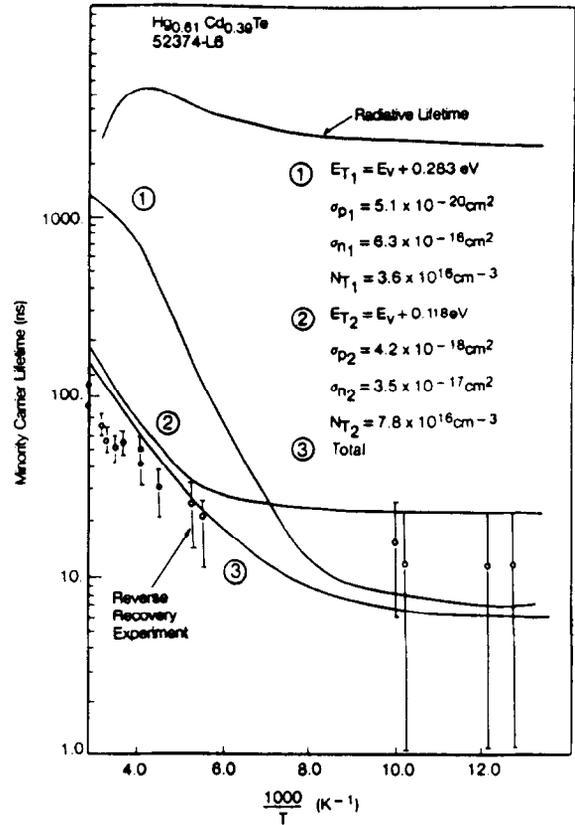Fig. 21. Position of the trap energy in p-$Hg_{1-x}Cd_xTe$ deduced by lifetime measurements as a function of temperature [100].

Fig. 22. Carrier lifetime as measured (circles) and as calculated from parameters determined by DLTS in p-$Hg_{1-x}Cd_xTe$ for the trap at $\frac{3}{4}\varepsilon_g$, curve (1); for the trap at $\sim \varepsilon_g/2$, curve (2); and for the two combined, curve (3) [76].

There were not many attempts to calculate the carrier lifetime in $Hg_{1-x}Cd_xTe$-based quantum confinement structures. However, calculations [75] have shown that the Auger recombination rate increases in $Hg_{1-x}Cd_xTe$ quantum wires as compared to quantum wells with similar width, but the rate is reduced significantly in quantum boxes. The calculated values of τ are much greater than the bulk Auger lifetime in the material with similar ε_g and doping level, but regrettably, the approximations made during the calculations [75] introduce errors in the absolute values of the calculated recombination rates and so one cannot directly compare the results with other data.

In the experimental papers cited above in this section, only the bulk recombination processes were observed in thin films. But there are also numerous observations of the recombination at surfaces, dislocations and other nonuniformities, in thin films as well as in the bulk crystals. We will discuss them in a separate section.
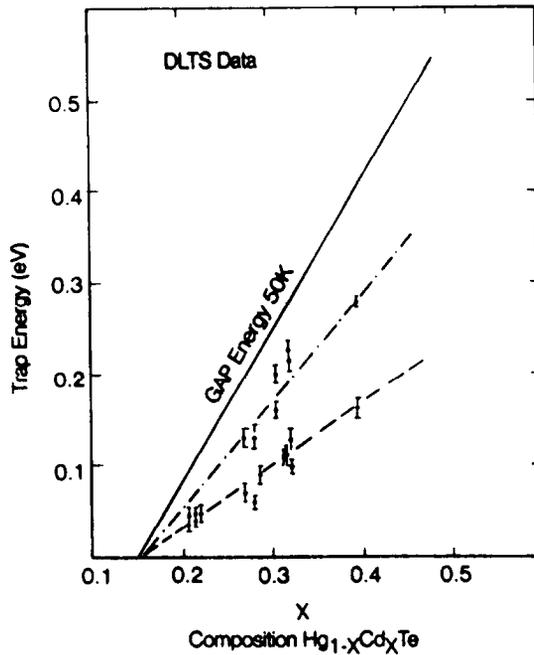
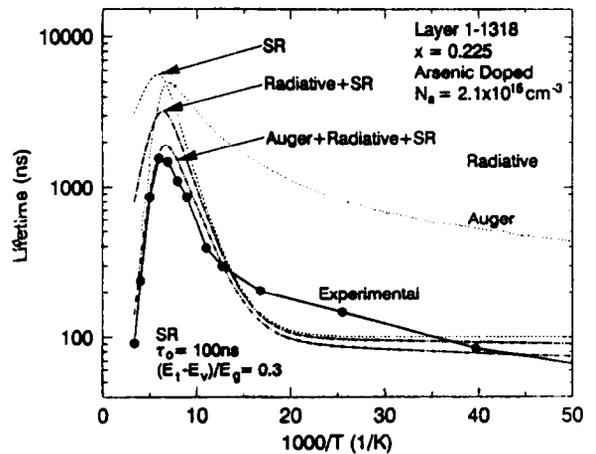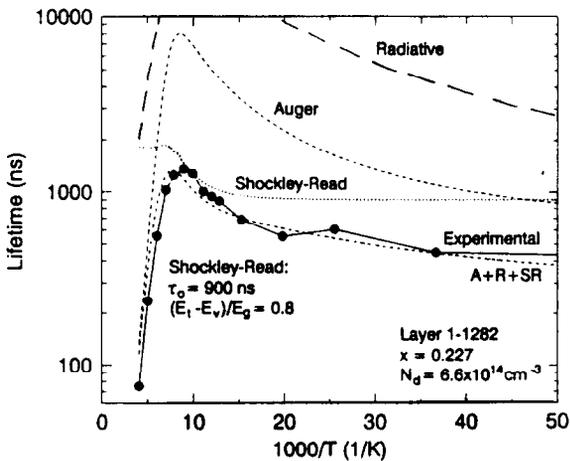Fig. 23. Trap energies in p-$Hg_{1-x}Cd_xTe$ determined by DLTS [76].

Fig. 24. Temperature dependence of the minority carrier lifetime of n-type MOCVD $Hg_{1-x}Cd_xTe$ on GaAs. Theoretical lifetimes for three recombination mechanisms used for data fitting are also shown separately and in combination [134].

Fig. 25. Temperature dependence of the minority carrier lifetime of p-type MOCVD $Hg_{1-x}Cd_xTe$ on GaAs. Theoretical lifetimes for three recombination mechanisms used for data fitting are also shown separately and in combination [134].

Table 1
Surface and interface recombination velocities in $Hg_{1-x}Cd_xTe$ on different surfaces and interfaces

Growth method[a]	Surface	Recombination velocity (cm/s)	Reference
SSR	Free surface, chemical etching	300–500	[64]
SSR	Free surface, plasma anodation	900–1500	[64]
LPE	Free surface, chemical etching	1000–5000	[64]
LPE	ZnS interface	2000–4000	[64]
LPE	LPE CdTe interface Surface coated with amorphous $(70\%ZnS + 30\%CaF_3)$	1000–20000 5000	[64] [4]

[a] SSR, solid state recrystallization; LPE, liquid phase epitaxy.

3.7. Recombination at macroscopic nonuniformities and dislocations

Let us now consider the influence of macroscopic nonuniformities and extended defects upon carrier lifetime in $Hg_{1-x}Cd_xTe$. The important kinds of nonuniformity that are always present in a sample are surfaces and interfaces. The recombination rate increases near a surface [124, 10], which may be connected either with recombination through surface levels or with gap reduction at the surface due to change in alloy composition that usually takes place in this region [117]. In Table 1 one can find the measured surface recombination velocities for specimens with $x \approx 0.2$ at $T = 77\,K$ (bulk carrier lifetimes were of the order of 1 μs). Some additional data can be found in Ref. [86].

For other temperatures S may be significantly different. In Ref. [26] it was found that

$$\ln S \sim T$$

over the temperature interval 280 to 340 K, so that S varies from 1.2×10^4 to 3.3×10^4 cm/s. For lower temperatures (around 50 K) the temperature dependence of S has been studied [51], where an activation exponent was used to fit the data. However, the calculated activation energy itself was temperature dependent, varying from 2.3 meV at $T < 40\,K$ to 12.5 meV at $T > 50\,K$.

The recombination velocity at the interface depends not only on the neighbouring materials but also on the technique used for the fabrication of the structure. Whereas a relatively high S value was reported for the $Hg_{1-x}Cd_xTe/CdTe$ heterointerface grown by liquid-phase epitaxy [64] (see Table 1), no traces of interface recombination was found in HgTe/CdTe superlattices grown by photoassisted MBE [107].

Low angle boundaries between crystallites with slightly different orientation (of order of 1.5′) that are often present in crystalline material can also serve as an additional drain for nonequilibrium carriers. This occurs, actually, only when the density of the low angle boundaries is as high as 200–300 cm^{-1} [65], whereas in most crystals their density is lower, being of the order of

10–100 cm^{-1}. Even in crystals with the highest investigated density of the boundaries (300 cm^{-1}), carrier lifetime in the low temperature interval $T < 100$ K is reduced only by a factor of three in comparison with material with low boundary concentration (less than 10 cm^{-1}), and for higher temperatures the effect of low angle boundaries is further reduced. It is worth noting that for intermediate boundary concentration (~ 90 cm^{-1}), the lifetime slightly *increases* when their concentration is raised, so it is rather probable that the change in the density of the low angle boundaries is accompanied by changes in the system of Shockley–Read centers and the observed boundary density dependence of the lifetime is in fact a more complicated phenomenon.

Let us now turn to the data concerning the influence of dislocations on the recombination rate in $Hg_{1-x}Cd_xTe$. It was found in Refs. [128, 113, 66] that dislocations do not influence the carrier lifetime at the dislocation density N_d lower than $(2–5) \times 10^5$ cm^{-2} in n-type films and crystals with $x = 0.2–0.3$. Bulk lifetime at 77 K in these specimens was in the sub-microsecond range. At $N_d \geq 5 \times 10^5$ cm^{-2}, the lifetime decreased as N_d increased (Fig. 26). On the contrary, in similar films with bulk lifetime 0.5–2 µs and $\varepsilon_g = 0.1–0.25$ eV corresponding to the wavelength 4–10 µm no influence of dislocations on the lifetime was found for N_d up to 10^7 cm^{-2} [63]. Perhaps the origin of this contradiction is the connection between the densities of the dislocations and the point recombination centers, in analogy with the previous case.

Another source of macroscopic nonuniformity is the alloy composition fluctuations in the bulk. Their characteristics depend significantly upon growth conditions. The regions with increased Hg content, where the gap is reduced and the Auger recombination rate is hence enhanced, have the strongest influence upon lifetime. In Ref. [123], regions with Hg content up to 95% were found around Te inclusions 40–50 µm in diameter. According to the calculations, these inclusions may reduce the lifetime by one or two orders of magnitude, even if they are present in a concentration as low as 10^6 cm^{-3} [123].
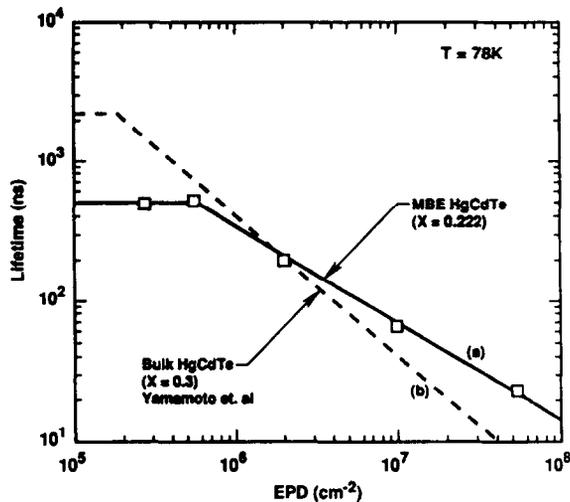

Fig. 26. Carrier lifetime measured at 78 K versus dislocation density [113]. Solid line, data from Ref. [113]; dashed line, data from Ref. [128]. The threading dislocation densities were obtained from the $Hg_{1-x}Cd_xTe$ layer etch-pit density (EPD) revealed by chemical etching.

4. Concluding remarks

One can see from the material presented above that interband transitions in narrow gap semiconductors can take place in different conditions and through different channels. Some of them were studied in more detail, others attracted less attention. From the theoretical point of view, the intrinsic recombination processes, the Auger recombination and radiative transitions, are more transparent, whereas recombination through states of different defects and surface recombination in narrow gap materials are almost uninitiated fields for theorists. From the point of view of experiment, the situation looks different. For example, the parameters of the main recombination centers in $Hg_{1-x}Cd_xTe$ have been found by many methods, but the experimental determination of the characteristics of the Auger transitions is rather difficult. The investigation of the recombination and impact ionization in narrow gap semiconductor-based size quantizing structures is only at its beginning. However considerable progress in the study of interband electron transitions in narrow gap semiconductors has taken place in recent years, especially in $Hg_{1-x}Cd_xTe$, and the number of articles devoted to this important problem is increasing. Hence one can look forward to further important results in this field in the future.

Acknowledgements

Appendix. Calculation of density matrices

Both the Kane and Lax models of band structure were obtained using the k–p method explicitly taking into account only the interaction between several states separated by the narrow energy gap (see, for example, Ref. [53]). As a result, the corresponding electron Hamiltonians are represented by matrices with a finite (and not large) number of rows and columns, m. We will show below how one can find the density matrices that describe mixed electron states that correspond to these Hamiltonians.

As a rule, the Hamiltonian $\hat{H}(k)$ of a model is known in the Luttinger–Kohn basis and so for $k \neq 0$ it is a non-diagonal matrix. Let us consider $\hat{H}$ in the basis of its own eigenfunctions (that are the Bloch waves) where it has the diagonal form

$$
\hat{H} = \begin{pmatrix}
\varepsilon_1(k) & 0 & 0 & 0 & \cdots & 0 & 0 \\
0 & \varepsilon_1(k) & 0 & 0 & \cdots & 0 & 0 \\
0 & 0 & \varepsilon_2(k) & 0 & \cdots & 0 & 0 \\
0 & 0 & 0 & \varepsilon_2(k) & \cdots & 0 & 0 \\
\vdots & \vdots & \vdots & & & & \vdots \\
0 & 0 & 0 & 0 & \cdots & \varepsilon_m(k) & 0 \\
0 & 0 & 0 & 0 & \cdots & 0 & \varepsilon_m(k)
\end{pmatrix}
\tag{A1}
$$

where the subscripts $1, 2, \ldots, m$ denote different bands, and each band has two branches due to Kramers degeneracy.

For simplicity, let us consider $m = 3$ so that

$$
\hat{H} = \begin{pmatrix}
\varepsilon_1(\boldsymbol{k}) & 0 & 0 & 0 & 0 & 0 \\
0 & \varepsilon_1(\boldsymbol{k}) & 0 & 0 & 0 & 0 \\
0 & 0 & \varepsilon_2(\boldsymbol{k}) & 0 & 0 & 0 \\
0 & 0 & 0 & \varepsilon_2(\boldsymbol{k}) & 0 & 0 \\
0 & 0 & 0 & 0 & \varepsilon_3(\boldsymbol{k}) & 0 \\
0 & 0 & 0 & 0 & 0 & \varepsilon_3(\boldsymbol{k})
\end{pmatrix} . \tag{A2}
$$

Our goal is to find the density matrix that describes the carrier state in the band i that contains the states from both branches in equal portions. Let us take $i = 1$ as an example. It is evident that in the basis of the eigenfunctions

$$
\rho_1(\boldsymbol{k}) = \frac{1}{2} \begin{pmatrix}
1 & 0 & 0 & 0 & 0 & 0 \\
0 & 1 & 0 & 0 & 0 & 0 \\
0 & 0 & 0 & 0 & 0 & 0 \\
0 & 0 & 0 & 0 & 0 & 0 \\
0 & 0 & 0 & 0 & 0 & 0 \\
0 & 0 & 0 & 0 & 0 & 0
\end{pmatrix} . \tag{A3}
$$

However, one cannot simply substitute this expression for ρ in Eq. (7), because the bases of the eigenfunctions are different for different $\boldsymbol{k}$. Hence one needs either to reduce all the expressions for the density matrices to a common basis or to build an expression for ρ which will be independent of the choice of basis. We will use the second idea and build the expression for ρ in tensor form.

It is clear from Eq. (A2) that the matrix

$$
\hat{H}(\boldsymbol{k}) - \varepsilon_3(\boldsymbol{k})\hat{I} ,
$$

where $\hat{I}$ is the unit matrix, has two diagonal matrix elements in place of $\varepsilon_3(\boldsymbol{k})$ (in the eigenfunction basis). Consequently, the matrix

$$
(\hat{H}(\boldsymbol{k}) - \varepsilon_2(\boldsymbol{k})\hat{I})(\hat{H}(\boldsymbol{k}) - \varepsilon_3(\boldsymbol{k})\hat{I})
$$

has non-zero matrix elements only at the two upper places on the main diagonal so it differs from $\hat{\rho}$ (Eq. (A3)) only by a multiplier. This means that $\hat{\rho}$ can be expressed as

$$
\hat{\rho}(\boldsymbol{k}) = \frac{(\hat{H}(\boldsymbol{k}) - \varepsilon_2(\boldsymbol{k})\hat{I})(\hat{H}(\boldsymbol{k}) - \varepsilon_3(\boldsymbol{k})\hat{I})}{\mathrm{Sp}\{(\hat{H}(\boldsymbol{k}) - \varepsilon_3(\boldsymbol{k})\hat{I})(\hat{H}(\boldsymbol{k}) - \varepsilon_3(\boldsymbol{k})\hat{I})\}} \tag{A4}
$$

so that $\mathrm{Sp}\,\hat{\rho} = 1$ as it should be.

The generalization of this procedure and formula (A4) to arbitrary i and m is straightforward. The expressions for $\hat{\rho}$ obtained in this way are not connected with any particular basis and can be immediately used for the calculation of the overlap integrals.

Practically, it is more convenient to use them in the Luttinger–Kohn basis, because the expression for the Hamiltonian is known just in that basis and $\hat{I}$ is invariant to the choice of basis.

In the Kane band model the expressions for the overlap integrals that are used in the Auger transition rate calculations are as follows [55, 57]

$$I_{cc}(k, q) = \mathrm{Sp}\{\rho_c(k)\rho_c(q)\} =$$

$$= \frac{1}{4}\left\{2\left[\varepsilon_g^2 + \frac{4}{3}(kq)P^2\right] - 2\varepsilon_g[\varepsilon_1(k) + \varepsilon_1(q)] + \varepsilon_1(k)\varepsilon_1(q)\left[\frac{5}{2} + \frac{3(kq)^2}{2k^2q^2}\right]\right\}$$

$$\times \left(\varepsilon_g^2 + \frac{8}{3}k^2P^2\right)^{-1/2}\left(\varepsilon_g^2 + \frac{8}{3}q^2P^2\right)^{-1/2}, \tag{A5}$$

$$I_{ch}(k, q) = \mathrm{Sp}\{\rho_c(k)\rho_h(q)\} = \frac{[k \times q]^2 P^2}{4q^2\varepsilon_c(k)\sqrt{\varepsilon_g^2 + \frac{8}{3}k^2P^2}}, \tag{A6}$$

$$I_{lh}(k, q) = \mathrm{Sp}\{\rho_l(k)\rho_h(q)\} = \frac{3[k \times q]^2\varepsilon_c(k)}{8k^2q^2\sqrt{\varepsilon_g^2 + \frac{8}{3}k^2P^2}}, \tag{A7}$$

$$D(k, q_1, q, q_2) = \mathrm{Sp}\{\rho_l(k)\rho_h(q_1)\rho_c(q)\rho_h(q_2)\}$$

$$= \frac{9\varepsilon_c(k)[\varepsilon_g - \varepsilon_c(q)]}{256[(\varepsilon_g^2 + \frac{8}{3}q^2P^2)(\varepsilon_g^2 + \frac{8}{3}k^2P^2)]^{1/2}}$$

$$\times \left\{1 + \frac{(q_1q_2)^2}{q_1^2q_2^2} + \frac{(kq)^2}{k^2q^2} - \frac{(q_1k)^2}{q_1^2k^2} - \frac{(kq_2)^2}{k^2q_2^2} - \frac{(qq_2)^2}{q^2q_2^2} - \frac{(q_1q)^2}{q_1^2q^2}\right.$$

$$\left. + \frac{(kq_1)^2(qq_2)^2 + (kq_2)^2(qq_1)^2 - (kq)^2(q_1q_2)^2}{k^2q^2q_1^2q_2^2}\right\}. \tag{A8}$$

Here k, q, q_1 and q_2 are the momenta of electrons; the subscripts c, l and h denote the conduction, light hole and heavy hole band, respectively; the energies are calculated from the top of the valence band so that $\varepsilon_{c\,min} = \varepsilon_g$; P is the Kane matrix element (see Eq. (30)).

References

[1] Abakumov V.N., Perel V.I., Yassievich I.N. 1978, Fiz. Tekh. Poluprovodn., 12, 3.
[2] Abakumov V.N., Merkulov I.A., Perel V.I., Yassievich I.N. 1985, J. Eksp. Teor. Fiz., 89, 1472.
[3] Adomaitis E., Grigoras K., Krotkus A. 1990, Semicond. Sci. Technol., 5, 836.
[4] Agamirova L.M., Movsum-zade A.A., Zaporozhchenko V.I., Rakhovskii V.I. 1991, Izvestiya AN SSSR: Neorg. Mater., 27, 628.
[5] Allegre J., Calas J. 1982, J. Cryst. Growth, 59, 338.
[6] Allegre J., Calas J., Fau C. 1982, Infrared Phys., 22, 65.
[7] Andersen W.W. 1980, Infrared Phys., 20, 363.

[8] Andrukhiv M.G., Mal'tseva V.A., Ivanov-Omskii V.I., Ogorodnikov V.K., Totieva T.Ts. 1979, Fiz. Tekh. Poluprovodn., 13, 362.
[9] Auth J., Genzow D., Herrmann K.H. 1977, Photoelektrische Erscheinungen (Akademie, Berlin).
[10] Bajaj J., Shin S.H., Pasko J.G., Khoshnevisan M. 1983, J. Vac. Sci. Technol. A, 1, 1749.
[11] Baraff G.A. 1962, Phys. Rev. 128, 2507.
[12] Barton S., Capper P., McAllister A., Jones C.J., Metcalfe N. 1993, Semicond. Sci. Technol., 8, S81.
[13] Bazhenov N.L., Gelmont B.L., Ivanov-Omskii V.I., Mal'kova A.A., Ogorodnikov V.K., Totoieva T. 1982, Fiz. Tekh. Poluprovodn., 16, 109.
[14] Beattie A.R. 1962, J. Phys. Chem. Solids, 23, 1049.
[15] Beattie A.R. 1987, Semicond Sci. Technol., 2, 281.
[16] Beattie A.R., Landsberg P.T. 1959, Proc. R. Soc. A, 249, 16.
[17] Beneslavskii S.D., Ivanov-Omskii V.I., Kolomiets B.T., Smirnov V.A. 1974, Fiz. Tverd. Tela, 16, 1620.
[18] Beneslavskii S.D., Dmitriev A.V. 1981, Solid State Commun., 39, 811.
[19] Bir G.L., Pikus G.E. 1972, Symmetry and Deformation Effects in Semiconductors (Nauka, Moscow) p. 303.
[20] Blakemore J.S. 1962, Semiconductor Statistics (Pergamon, Oxford).
[21] Blue M.D. 1964, Phys. Rev., 134, A226.
[22] Bogdanov E.V., Brandt N.B., Fleyshman L.S. 1983, Vestnik MGU: Ser. Fiz. Astronom., 24, 92.
[23] Bogdanov E.V., Brandt N.B., Fleyshman L.S. 1984, Fiz. Tekh. Poluprovodn., 18, 1021.
[24] Bogdanov E.V., Popov V.L., Fleyshman L.S. 1985, Fiz. Tekh. Poluprovodn., 19, 1929.
[25] Bogdanov E.V., Brandt N.B., Fleyshman L.S., Popov V.L. 1985, Solid State Commun., 53, 947.
[26] Bolgov S.S., Elizarov A.I., Malyutenko V.K., Savchenko A.P. 1991, Optoelektron. Poluprovodn. Tekh., No. 19, 58.
[27] Bonch-Bruevich V.L., Kalashnikov S.G. 1977, Semiconductor Physics (Nauka, Moscow).
[28] Brandt N.B., Svistova Ye.A., Svistov Ye.A., Yakovlev G.D. 1971, J. Eksp. Teor. Fiz., 61, 1078.
[29] Brennan K.F., Mansour N.S. 1991, J. Appl. Phys., 69, 7844.
[30] Bude J., Hess K., Iafrate C.J. 1992, Phys. Rev. B 45, 10958.
[31] Calas J., Allegre J. 1982, Phys. Status Solidi (b), 112, 179.
[32] Calas J., Allegre J., Fau C. 1981, Phys. Status Solidi (b), 107, 275.
[33] Cancen G.L., Schmit J.L., Casselman T.N. 1982, J. Appl. Phys., 53, 7099.
[34] Casselman T.N. 1982, Lect. Notes Phys., 152, 147.
[35] Casselman T.N., Petersen P.E. 1981, Solid State Commun., 39, 1117.
[36] Chen M.C., Goodwin M.V., Polygreen T.L. 1988, J. Cryst. Growth, 86, 484.
[37] Chen Y.-Z., Tang T.-W. 1989, J. Appl. Phys., 65, 4279.
[38] Cho S.M., Lee H.H. 1992, J. Appl. Phys., 71, 1298.
[39] Chu J., Xu Sh., Tang D. 1983, Appl. Phys. Lett., 43, 1064.
[40] Cotton V.A., Wilson J.A., Jones C.E. 1985, J. Appl. Phys., 58, 2208.
[41] Curbey R.C., Ferry D.K. 1973, Phys. Status Solidi (a), 15, 319.
[42] Dmitriev A.V. 1983, Fiz. Tekh. Poluprovodn., 17, 2222.
[43] Dmitriev A.V. 1990, Solid State Commun., 74, 577.
[44] Dmitriev A.V. 1990, Semicond. Sci. Technol., 5, 1.
[45] Dmitriev A.P., Mikhailova M.P., Yassievich I.N. 1987, Phys. Status Solidi (b), 140, 9.
[46] Krotkus A., Dobrovol'skis Z. 1988, Electrical Conductivity of Narrow Gap Semiconductors (Mokslas, Vilnius).
[47] Dornhaus R., Nimtz G. 1976, in: Solid State Physics, 76 (Springer, Berlin).
[48] Dumke W.P. 1968, Phys. Rev., 167, 783.
[49] Dyakonov M.I., Khaetskii A.V. 1980, Fiz. Tekh. Poluprovodn., 14, 1499.
[50] Ferry D.K., Barker J.R., Jacoboni C., eds., Physics of Nonlinear Transport in Semiconductors (Plenum, New York, 1980).
[51] Finkman E., Shaham S.E. 1989, J. Vac. Sci. Technol. A, 7, 464.
[52] Feynman R.P. 1972, Statistical Mechanics (Benjamin, Massachusetts) Ch. 6, § 7.
[53] Gantmakher V.F., Levinson I.B. 1987, Scattering of Current Carriers in Metals and Semiconductors (North-Holland, Amsterdam) Ch. 1.
[54] Gelmont B.L. 1978, Phys. Lett. A, 66, 323.

[55] Gelmont B.L. 1978, Zh. Eksp. Teor. Fiz., 75, 536.

[56] Gelmont B.L. 1980, Fiz. Tekh. Poluprovodn., 14, 1913.

[57] Gelmont B.L. 1981, Fiz. Tekh. Poluprovodn., 15, 1316.

[58] Gelmont B.L., Ivanov-Omskii V.I., Maltseva V.A., Smirnov V.A. 1981, Fiz. Tekh. Poluprovodn., 15, 1109.

[59] Gelmont B.L., Ivanov-Omskii V.I., Maltseva V.A., Smirnov V.A. 1982, Lecture Notes in Physics, Vol. 152 (Springer, Berlin) p. 131.

[60] Gelmont B.L., Sokolova Z.N. 1982, Fiz. Tekh. Poluprovodn., 16, 1670.

[61] Gelmont B.L., Ki-Sang Kim, Shur M. 1992, Phys. Rev. Lett. 69, 1280.

[62] Gerhardts R.R., Dornhaus L., Nimtz G. 1978, Solid-State Electron., 21, 1467.

[63] Goodwin M.V., Kinch M.A., Koestner R.J. 1989, J. Vac. Sci. Technol. A, 7, 523.

[64] Graft R.D., Carlson F.F., Dinan J.H., Boyd P.R., Longshore R.E. 1983, J. Vac. Sci. Technol. A, 1, 1696.

[65] Grigoryev N.N., Ergakov V.K., Karachevtseva L.A., Kurbanov K.R., Lyubchenko A.V., Malovichko E.A. 1991, Fiz. Tekh. Poluprovodn., 25, 1649.

[66] Grigoryev N.N., Karachevtseva L.A., Kurbanov K.R., Lyubchenko A.V. 1991, Fiz. Tech. Poluprovodn., 25, 464.

[67] Hangleiter A. 1985, Phys. Rev. Lett., 55, 2976.

[68] Hangleiter A. 1987, Phys. Rev. 35, 9149.

[69] Hangleiter A. 1988, Phys. Rev. B, 37, 2594.

[70] Humphreys R.G. 1983, Infrared Phys., 23, 171.

[71] Humphreys R.G. 1986, Infrared Phys., 26, 337.

[72] Ivanov-Omskii V.I., Maltseva V.A., Britov A.D., Sivachenko S.D. 1978, Phys. Status Solidi (a), 46, 77.

[73] Ivanov-Omskii V.I., Kurbanov K.R., Maltseva V.A., Smirnov V.A., Yuldashev Sh.U. 1983, Fiz. Tekh. Poluprovodn., 17, 27.

[74] Ivanov-Omskii V.I., Kurbanov K.R., Rustamov R.B., Smirnov V.A., Yuldashev Sh.U. 1984, Fiz. Tekh. Poluprovodn., 18, 1509.

[75] Jiang Y., Teich M.C., Wang W.I., Meyer J.R. 1992, J. Appl. Phys., 71, 3394.

[76] Jones C.E., Nair V., Polla D.L. 1981, Appl. Phys. Lett., 39, 248.

[77] Jones C.E. et al. 1985, J. Vac. Sci. Technol. A, 3, 131.

[78] Kane E.O. 1957, J. Phys. Chem. Solids, 1, 249.

[79] Keldysh L.V. 1963, Sov. Phys. – JETP, 21, 1135.

[80] Laks D.B., Neumark G.F., Hangleiter A., Pantelides S.T. 1988, Phys. Rev. Lett., 61, 1229.

[81] Landsberg P.T. 1991, Recombination in Semiconductors (Cambridge University Press, Cambridge).

[82] Lax M. 1960, Phys. Rev., 119, 1502.

[83] Lévêque G., Nasser M., Bertho D., Orsal B., Alabedra R. 1993, Semicond. Sci. Technol., 8, 1317.

[84] Littler C.L., Song X.N., Yu Z., Elkind J.L., Lowney J.R., Seiler D.J. 1993, Semicond. Sci. Technol., 8, S317.

[85] Landau L.D., Lifshits E.M. 1977, Quantum Mechanics: Non-Relativistic Theory 3rd Ed. (Pergamon, Oxford).

[86] Lopes V.C., Sillaios A.J., Chen M.C. 1993, Semicond. Sci. Technol., 8, 824.

[87] Lifshits E.M., Pitayevskii L.P. 1980, Statistical Physics, Vol. 2: Condensed Matter Theory (Pergamon, Oxford).

[88] Lui W.W., Yoshikuni Yu., Yamanaka T., Yokoyama K. 1993, J. Appl. Phys., 73, 1226.

[89] Man P., Pan D.S. 1991, Phys. Rev. B, 44, 8745.

[90] Manankov V.M. 1982, Ph.D. Thesis, Moscow State University, Moscow.

[91] Merilainen C.A., Jones C.E. 1983, J. Vac. Sci. Technol. A, 1, 1637.

[92] Meshkov S.V. 1985, J. Eksp. Teor. Fiz., 89, 1734.

[93] Mikheev V.M., Pomortsev R.V. 1977, Fiz. Tekh. Poluprovodn., 11, 908.

[94] Mocker M., Ziep O. 1983, Phys. Status Solidi (b), 115, 415.

[95] Mukhitdinov A.M., Stafeev V.I. 1992, Fiz. Tekh. Poluprovodn., 26, 1830.

[96] Niedziela T., Rogalski A., Piotrovskii J. 1988, Infrared Phys., 28, 311.

[97] Nimtz G., Bauer G., Dornhaus R., Müller K.H. 1974, Phys. Rev. B, 10, 3302.

[98] Nimtz G. 1980, Phys. Reports, 63, 266.

[99] Nimtz G., Schlicht B. 1983, in: Narrow-Gap Semiconductors, ed. G. Höhler, Springer Tracts in Modern Physics, Vol. 98 (Springer, Berlin).

[100] Polla D.L., Tobin S.P., Reine M.B., Sood A.K. 1981, J. Appl. Phys., 52, 5182.

[101] Polla D.L., Aggarwal R.L., Nelson D.A., Shanley J.F., Reine M.B. 1983, Appl. Phys. Lett., 43, 941.
[102] Popov V.L. 1983, Fiz. Tverd. Tela, 25, 2127.
[103] Pratt R.G., Hewett J., Capper P., Jones C.L., Judd N. 1986, J. Appl. Phys., 60, 2377.
[104] Pratt R.G., Hewett J., Capper P., Jones C.L., Quelch M.J. 1983, J. Appl. Phys., 54, 5152.
[105] Quade W., Rossi F., Jacoboni C. 1992, Semicond. Sci. Technol., 7, B502.
[106] Reggiani L., ed., Hot Electron Transport in Semiconductors, Topics in Applied Physics, Vol. 58 (Springer, Berlin, 1985).
[107] Reisinger A.R., Harris K.A., Myres T.H., Yanka R.W., Mohnkern L.M., Hoffman C.A. 1992, Appl. Phys. Lett., 61, 699.
[108] Ridley B.K. 1983, J. Phys. C, 16, 3373.
[109] Robbins D.J. 1980, Phys. Status Solidi (b), 97, 9; 98, 11.
[110] Rosman R., Katzir A. 1982, IEEE J. Quant. Electron., QE-18, 814.
[111] Schacham S.E., Finkman E. 1985, J. Appl. Phys., 57, 2001.
[112] Schilz J., Nimtz G., Geibel C., Ziegler J. 1988, J. Cryst. Growth, 86, 677.
[113] Shin S.H., Arias J.M., Zandian M., Pasko J.G., DeWames R.E. 1991, Appl. Phys. Lett., 59, 2718.
[114] Shockley W. 1961, Solid-State Electron., 2, 35.
[115] Smith R.A. 1978, Semiconductor Physics 2nd Ed. (Cambridge University Press, Cambridge).
[116] de Souza M.E., Boukerche M., Faurie J.P. 1990, J. Appl. Phys., 68, 5195.
[117] Takita K., Ipposhi T., Murakami K., Masuda K., Kudo H., Seki S. 1986, J. Appl. Phys., 59, 1500.
[118] Takita K., Ipposhi T., Masuda K. 1987, Solid State Commun., 61, 817.
[119] Tennant W.E., Cockrum C.A., Gilpin J.B., Kinch M.A., Reine M.B., Ruth R.P. 1992, J. Vac. Sci. Technol. B, 10, 1359.
[120] Townsend J.C. 1910, Theory of Ionization of Gases by Collision, Oxford.
[121] Trifonov V.I., Martyakhin V.A., Stukan V.A., Zaets N.F. 1978, Fiz. Tekh. Poluprovodn., 12, 1641.
[122] Tsidilkovskii I.M., Kharus G.I., Shelushinina N.G. 1985, Adv. Phys., 34, 43.
[123] Vlasenko A.I., Gavrilyuk Yu.N., Lyubchenko A.V., Sal'kov E.A. 1979, Fiz. Tekh. Poluprovodn., 13, 2180.
[124] Vlasenko A.I., Lyubchenko A.V., Sal'kov E.A. 1980, Ukrainian Fiz., 25, 434.
[125] Voitsekhovskii A.V., Lilenko Yu.V. 1981, Phys. Status Solidi (a), 67, 381.
[126] Wilson S.R., Brand S., Beattie A.R., Abram R.A. 1993, Semicond. Sci. Technol., 8, 1546.
[127] Wolf P.A. 1954, Phys. Rev., 95, 1415.
[128] Yamamoto T., Miyamoto Y., Tanikawa K. 1985, J. Cryst. Growth, 72, 270.
[129] Yuan H., Tong F., Tang D. 1993, Opt. Eng., 32, 608.
[130] The physical basis of DLTS in application to the narrow gap materials can be found in the article: Zachman S.J., Finkman E., Bahir G. 1993, Semicond. Sci. Tecnol., 8, S90.
[131] Ziep O., Mocker M. 1980, Phys. Status Solidi (b), 98, 133.
[132] Ziep O., Genzow D., Mocker M., Herrmann K.H. 1980, Phys. Status Solidi (b), 99, 129.
[133] Ziep O., Mocker M., Genzow D., Herrmann K.H. 1978, Phys. Status Solidi (b), 90, 197.
[134] Zucca R., Edwall D.D., Chen J.S., Johnston S.L., Younger C.R. 1991, J. Vac. Sci. Technol. B, 9, 1823.